

Title Page

Human β -Amyloid 40 (hA β ₄₀) Kinetics after Intravenous (IV) and Intracerebroventricular (ICV) Injections and Calcitriol Treatment in Rats *in vivo*

H. Benson Peng, Keumhan Noh, Sophie R. Pan, Victor Saldivia, Sylvia Serson, Anja Toscan,
Inés A.M. de Lannoy[†], and K. Sandy Pang[†]

[†]co-senior authors

Department of Pharmaceutical Sciences (H.B.P., K.N., K.S.P.), Leslie Dan Faculty of Pharmacy,
University of Toronto

and

InterVivo Solutions Inc. (V.S., S.R.P., S.S., A.T., I.A.L.), Mississauga, Ontario, Canada

Running Title Page

Running Title: hA β ₄₀ Kinetics with Calcitriol Induction of P-gp in Rats

Correspondence:

Dr. K. Sandy Pang

Leslie Dan Faculty of Pharmacy, University of Toronto

144 College Street, Toronto, Ontario

Canada M5S 3M2

TEL: 416-978-6164

FAX: 416-978-8511

E-mail: ks.pang@utoronto.ca

Text pages: 21

Tables: 4

Figures: 7

Abstract: 222 words

Introduction: 750 words

Discussion: 1442 words

References: 71

Abbreviations: AD, Alzheimer's disease; AUC, area under the concentration-time curve; BAB, blood-arachnoid barrier; BBB, blood-brain barrier; BCSFB, blood-CSF barrier; CSF, cerebrospinal fluid; CM, cisterna magna; hA β ₄₀, human amyloid-beta 40; ICV, intracerebroventricular; IP, intraperitoneal; IV, intravenous; LV, lateral ventricle; Lrp1, low density lipoprotein receptor-related protein 1; Mrp1, multidrug resistance-associated protein 1; P-gp, P-glycoprotein; PK, pharmacokinetics; SDB, Standard Dilution Buffer; subarachnoid space, SAS

Abstract

Amyloid- β peptides of 40 and 42 amino acid lengths, which are synthesized in neurons and degraded in the brain and liver, have the potential to aggregate and form neuritic plaques in Alzheimer's disease (AD). The kinetics of human A β_{40} (hA β_{40}) was examined in the rat pursuant to intravenous (IV) and intracerebroventricular (ICV) administration after pretreatment with calcitriol, the active vitamin D receptor ligand [6.4 nmol·kg⁻¹ in 0.3 mL corn oil every other day for 4 intraperitoneal (IP) doses] to induce P-glycoprotein (P-gp) and enhance hA β_{40} brain efflux. The interference of hA β_{40} by media matrix that suppressed absorbance readings in the ELISA assay was circumvented with use of different calibration curves prepared in Standard Dilution Buffer, undiluted, 10-10,000 or 5-fold diluted plasma, or artificial cerebrospinal fluid. Simultaneous fitting of hA β_{40} plasma and CSF data after IV and ICV administration were described by catenary-mammillary models comprising of a central and two peripheral compartments, the brain, and one to four CSF compartments. The model with only one CSF compartment (Model I) best fitted the IV data that showed a faster plasma decay $t_{1/2}$ and slower equilibration between plasma and brain/CSF. Calcitriol induction increased the brain efflux rate constants, k_{41} (1.8-fold) at the blood-brain barrier (BBB), when compared to the control group, as confirmed by the 2-fold ($P < 0.05$) increase in brain P-gp relative protein expression.

Significance Statement

An accurate description of the kinetic behavior of hA β ₄₀, is needed in defining the toxic peptide as a biomarker of Alzheimer's disease. Modeling of hA β ₄₀ data after intravenous and intracerebroventricular administration to the rat revealed an initially faster plasma half-life that reflects faster peripheral distribution but slower equilibration between plasma and brain/CSF; with calcitriol pretreatment, which increased P-gp protein expression in brain, clearance was enhanced for hA β ₄₀ efflux from brain.

Introduction

Amyloid- β ($A\beta_{40}$ and $A\beta_{42}$) of 40 and 42 amino acid lengths are formed via sequential cleavage of the amyloid precursor protein (APP) by β - and γ -secretases in neurons (Haass et al., 1992; Hartman et al., 1997; Weidemann et al., 1999). These pathogenic peptides are precursors of plaque formation in Alzheimer's disease, AD (Hardy and Higgins, 1992), and contribute to the amyloid cascade hypothesis that centers on the concept that $A\beta$ toxicity in brain is pivotal to AD pathology (Zlokovic et al., 2000). In humans, the fractional synthesis and clearance of $A\beta$ are 7.6% and 8.3% per h, respectively (Bateman et al., 2006). The average $A\beta$ production rate (6.6% - 6.8% per h) by β -secretase (BACE1) is similar between normal and AD subjects, whereas brain $A\beta$ clearance is much lower for those diagnosed with AD (~5.2% per h) compared to normal subjects (7.0-7.6% per h) (Mawuenyega et al., 2010). $A\beta$ clearance across the BBB is 6-fold higher than the interstitial fluid bulk flow (Bell et al., 2007) and 2-fold higher than metabolism by neprilysin, the proteolytic enzyme in the microglia that degrades $A\beta_{40}$ (Iwata et al. 2000, Qosa et al., 2014). $A\beta_{40}$ clearance is construed as injection-site specific since ^{125}I - $A\beta_{40}$ and ^{14}C -sucrose injected into the lateral ventricles of rat brains were found to be rapidly distributed throughout the CSF and cleared into blood while diffusion into brain tissue (parenchyma) was poor and negligible (Gheri-Egea et al., 1996a; 1996b). About 62% of ^{125}I - $A\beta_{40}$ injected intracerebrally to the mouse brain is found effluxed across the BBB, while the remaining 38% was associated with degradation and CSF bulk flow (Qosa et al., 2014). These processes appear to be $A\beta_{40}$ - or $A\beta_{42}$ -dependent, since radiolabeled $A\beta_{40}$ injected into the hippocampus is readily transported across the BBB (Iwata et al., 2000) to reach the liver for elimination (Ghiso et al., 2004; Tamaki et al., 2006), whereas radiolabeled $A\beta_{42}$ injected into the hippocampus lingered and was mostly recovered in the brain (Iwata et al., 2005).

The efflux of $A\beta$ peptides from the brain via the blood-brain barrier (BBB) and blood-cerebrospinal fluid barrier (BCSFB) to the peripheral circulation allows the peptides to reach peripheral degradation organs, namely the liver (Ghiso et al., 2004; Tamaki et al., 2006) and potentially the kidney

(Yasojima et al., 2001). Currently, there is strong evidence that the liver is a major organ that contributes to A β peptide degradation (Marques et al., 2009; Maarouf et al., 2018). An imbalance of A β peptide accumulation and degradation in brain or liver, or efflux from the brain across the BBB and BCSFB could contribute to the seeding effect, allowing for accumulation, aggregation, and insoluble senile plaque formation (Shibata et al., 2000; Zlokovic et al., 2000; Bates et al., 2009; Deane et al., 2009).

Currently, there has not been any cohesive description of hA β ₄₀ kinetics. A β pharmacokinetic studies are scarce and the results have been spurious. Different half-lives ($t_{1/2}$ s) of 2.5 to 3 min (Ghisso et al., 2004), 0.7 to 1.7 h (Abramowski et al., 2008), 2 h (Cirrito et al., 2003), and some ranging from 26 to 240 min (Shibata et al., 2000) have been reported in mice *in vivo*. The disparity in the $t_{1/2}$'s is likely due to inappropriate methodology (inadequate sampling or use of total radioactivity to represent A β), misinterpretation, aggregation problems of A β (Teplow, 2006), and/or interference in the enzyme-link immunosorbent assay (ELISA) (Lanz and Schachter, 2006). Whether CSF concentration is a good surrogate of the unbound brain concentration (Tang et al., 2009) and whether hA β ₄₀ or the ratio of hA β ₄₂/hA β ₄₀ in plasma or CSF relate to the extent of cerebral amyloidosis or AD progression (Seppala et al., 2010; Vergallo et al., 2019) are unknown. We initiated a study in rats with intravenous (IV) or intracerebroventricular (ICV) administration of hA β ₄₀ to appraise the complex kinetics of hA β ₄₀ after calcitriol treatment. The rat, a larger rodent that does not synthesize hA β ₄₀, was chosen for study since its size allows for sequential plasma and CSF sampling, and any variation in hA β ₄₀ synthesis is non-existent. A sound strategy that accounted for matrix interference by albumin, transthyretin, or α -2-macroglobulin that quench the A β signal (Biere et al., 1996; Kuo et al., 1999; Lanz and Schachter, 2006; Alemi et al., 2016) in the sample was used to assay for hA β ₄ in plasma and CSF. The pharmacokinetics of hA β ₄₀, a substrate of P-gp (Lam et al., 2001), was studied after pretreatment with calcitriol, active ligand of the vitamin D receptor, VDR, and known to induce for P-gp in humans, mice and rats (Durk et al., 2012; 2014).

Materials and Methods

Reagents and chemicals. All reagents, chemicals, and calcitriol in powder form were obtained from Sigma-Aldrich (Mississauga, ON). Powdered hA β ₄₀ peptide was purchased from Biopeptide Co., Inc. (San Diego, CA). The ELISA kit for the hA β ₄₀ (KHB3841) assay and the primary mouse anti-rat P-gp antibody (C219) were purchased from ThermoFisher Scientific (Mississauga, ON), whereas the rabbit anti-rat neprilysin antibody (AB5458) was from Millipore Sigma (Etobicoke, ON) and rabbit anti-Lrp1 antibody (ab92544) and mouse anti-rat Gapdh (ab8245) antibodies, from Abcam (Cambridge, MA). The rat anti-Mp1 antibody (MC-106) was from Kamiya Biomedical (Seattle, WA). The goat anti-mouse or goat anti-rabbit IgG secondary antibody conjugated to horseradish peroxidase was procured from BioRad (Mississauga, ON). Artificial CSF (aCSF) was obtained from Harvard Apparatus (St. Laurent, QC).

Preparation of hA β ₄₀ stock solution for dosing. The hA β ₄₀ peptide for dosing was prepared according to previously described reports (Stine et al., 2003; Teplow 2006; Roychaudhuri et al., 2015). Briefly, the hA β ₄₀ in powder form was solvated in 100% 1,1,1,3,3,3-hexafluoro-2-propanol (HFIP) and made up to 1 mM (Stine et al., 2003) in the original glass vial, and left at room temperature until a clear solution was obtained. The content was transferred to a 1.5 mL polypropylene microcentrifuge tube for evaporation of HFIP overnight in the fume hood. The clear peptide film was dried under vacuum in a SpeedVac rotary evaporator for 2 h to ensure complete HFIP removal, and the resulting desiccated peptide film was re-dissolved in 10% (v/v) 0.06 N NaOH, 45% (v/v) ddH₂O, and 45% (v/v) phosphate buffer solution (PBS, 20 mM sodium phosphate, pH = 7.4) to a 1 mg·mL⁻¹ stock solution. This reconstituted hA β ₄₀ peptide stock solution was sonicated over an ice bath (Branson) for 1 min then aliquoted and stored immediately at -80 °C for future use. The preparation and storage of hA β ₄₀ in this fashion ensured that the peptide was stable and reproducible for IV and ICV administration. The integrity and stability of the 1 mg·mL⁻¹ hA β ₄₀ stock solution stored at -80°C up to a month was ascertained on different occasions with ELISA assay and a LC-MS/MS procedure developed at InterVivo Solutions. Briefly, an AB Sciex 6500QTrap mass

spectrometer with Exion LC system and autosampler, a Thermo ProSwift RP-4H column, and gradient elution (mobile phase A: 0.3% NH₄OH in water, mobile phase B: acetonitrile at 0.4 mL/min) was used over a run time of 4.7 min. The mass spectrometer was operated with a TIS interface and multiple reaction monitoring in positive ion mode. Ion transitions that were used for quantitation were: hAβ₄₀ m/z 1083.3 (M+4H)⁴⁺ → 1054.2 with ¹⁵N-Aβ₄₀ (m/z 1096.3 (M+4H)⁴⁺ → 1066.9) as internal standard. hAβ₄₀ was shown to be stable with 1-4 freeze-thaws. For IV dosing, the 1 mg·mL⁻¹ stock solution was further diluted with PBS (1:4, v/v, pH 7.4 from GIBCO, obtained from ThermoFisher Scientific, catalog number, 10010023) on the day of the experiment, whereas for ICV dosing, the desiccated peptide film was used to prepare a 2 mg·mL⁻¹ solution for administration. The concentrations of the IV and ICV doses were first estimated by ultraviolet (UV) spectrophotometry (UV-1700, Shimadzu Scientific Instruments, Columbia, Maryland) at the wavelength of 280 nm due to the single Tyr residue present on the hAβ₄₀ peptide (Jan et al., 2010), and concentration of the dosing solution was subsequently confirmed by ELISA. **ELISA.** The primary 160 ng standard stock of hAβ₄₀, provided in the kit by the manufacturer, was first dissolved with 1.6 mL of the Standard Reconstitution Buffer (55 mM sodium bicarbonate, pH 9) to obtain a 100 ng·mL⁻¹ stock solution. This stock solution was diluted to 10,000 pg·mL⁻¹ with the Standard Dilution Buffer (SDB) to prepare the 8 standards by serial dilution (500 to 7.81 pg·mL⁻¹), according to the protocol suggested by the manufacturer. The absorbances of the standards were measured at 450 nm (SpectraMax 340PC; Molecular Devices, Sunnyvale, CA) for construction of the calibration curve for the determination of plasma or CSF concentrations.

The presence of albumin, transthyretin, or α-2-macroglobulin could quench the Aβ signal and interfere with the ELISA assay for hAβ₄₀ in plasma and CSF (Biere et al., 1996; Kuo et al., 1999; Lanz and Schachter, 2006; Alemi et al., 2016). The interference from plasma was examined by varying the proportion of rat plasma (from 0% to 95% plasma) in the hAβ₄₀ standards, prepared as 1,000, 2,000, 5,000 and 8,000 pg·mL⁻¹ (n = 3 in each set). Also, different media were used to prepare the standards of various

calibration curves. The CSF standards were prepared in SDB (0, 10 to 10,000-fold, v/v) or aCSF or directly loaded as 50 μ L aliquots onto the ELISA plate. The interference from rat plasma or aCSF was examined among calibration curves generated from undiluted blank plasma (50 μ L direct loading), 5- and 10-10,000-fold diluted plasma in SDB, or in 100% aCSF vs. the calibration curve based on hA β ₄₀ standards prepared in SDB.

In vivo experiments. All animal protocols were approved by the InterVivo Solutions Animal Care Committee and studies were carried out in accordance with the principles of the Canadian Council on Animal Care. Male Sprague-Dawley rats, purchased from Charles River Laboratories (St. Constant, QC), were acclimated under a 12 h light/dark cycle and given water and chow *ad libitum* at InterVivo Solutions for at least 5 days prior to dosing. The rats (318 ± 41.6 g) were weighed on the day of dosing.

The effect of corn oil, the vehicle for intraperitoneal (IP) injection of calcitriol, on hA β ₄₀ kinetics was first investigated in absence of calcitriol. The hA β ₄₀ dose was determined after a broad and exhaustive literature search on A β injections via intravenous, intracerebral or intracerebroventricular routes to various animal (guinea pigs, mice, and rats) models. In the first set of animals, the hA β ₄₀ dose (68.5 ± 12.0 μ g·kg⁻¹; $n = 4$) was administered IV to rats that were pretreated blank corn oil (0.3 mL), given every other day IP for 4 doses, for comparison of hA β ₄₀ kinetics (64.5 ± 13.2 μ g·kg⁻¹ in saline, $n = 12$) among control rats that were not pretreated with corn oil. In the second set of rats, hA β ₄₀ kinetics following a single hA β ₄₀ ICV dose (48.0 ± 14.9 μ g·kg⁻¹ in corn oil, $n = 4$) were compared to those after IV dosing (data from first set, combined; $n = 16$, since corn oil did not affect hA β ₄₀ kinetics). For the last set, rats were pretreated with calcitriol (6.4 nmol·kg⁻¹ in 0.3 mL corn oil, every other day for 4 doses, intraperitoneally, IP), then administered a single IV (73.5 ± 6.02 μ g·kg⁻¹; $n = 7$) or ICV (20.3 ± 1.30 μ g·kg⁻¹; $n = 5$) dose of hA β ₄₀ one day after completion of the calcitriol pretreatment regimen.

Surgery was performed under 4% isoflurane in oxygen for anesthesia and 1-3% for maintenance and rats were allowed to fully recover for one day before dosing. Catheters were implanted into the jugular

vein for IV dosing or the lateral ventricle (LV) for ICV dosing, into the carotid artery for serial blood sampling, and into the cisterna magna (CM) for CSF collection. The common bile duct was cannulated for the collection of bile in 3 rats (IV control group) that remained anesthetized during dosing and sampling. For IV dosing, the jugular vein catheter (CX-2011S, BASi West Lafayette, IN) was prefilled with heparinized (40 U/mL) physiological saline solution to prevent blood coagulation. A hA β_{40} (~ 0.2 mL) bolus dose was injected into the jugular vein followed by flushing with ~ 0.1 mL of heparinized saline. For ICV dosing, an intracerebroventricular guide cannula (P1 technologies, Roanoke, VA) was placed into the right lateral ventricle of the brain (stereotactic coordinates: -0.92 AP, -1.3 L, and -3.1 DV relative to the bregma) with facilitation of a stereotaxic instrument. The dosing solution (0.01 mL) was administered via a 1 mL Hamilton glass microsyringe (ID 1.46 mm) fitted to the ICV injection catheter at $1 \mu\text{L} \cdot \text{s}^{-1}$ using a Harvard Apparatus Pump 11 elite system. Serial blood sampling (0.15 mL) was performed after both IV and ICV injections via the carotid artery catheter at times 0, 0.5, 1, 2, 5, 10, 15, 30, 45, 60, 90, 120, 150, and 180 min post-dose, and sampled volumes were replaced with heparinized saline. Plasma was obtained by immediate centrifugation of blood at 4,000x g for 10 min at 4 °C. For CSF sampling, a BSIL-T015 0.015ID tubing cannula (Plymouth Meeting, PA) was inserted into the cisterna magna and kept in place by a metal pin stopper (SP22/12), Serial CSF sampling (10-50 μL) was conducted via the cisterna magna cannula at times 0, 15, 30, 60, 120, and 180 min. A BASi CX-8000S catheter was inserted into the common bile duct for sampling (untreated IV injected saline-treated rats, n=3) at 30 min intervals. Urine was collected into pre-tared tubes throughout the 180 min of experimentation. After the last sample collection, rats were sacrificed by exsanguination under isoflurane anesthesia and transcardially perfused with 50 mL ice-cold physiological saline solution prior to tissue collection. Hemibrains, liver (minced), kidney, and all subsequent samples were flash frozen with liquid nitrogen, weighed and stored at -80 °C for future analysis.

Non-compartmental analysis. All plasma concentrations and amounts in bile or urine were normalized to dose and expressed as $\% \text{dose} \cdot \text{mL}^{-1}$ (frequency) and $\% \text{dose}$, respectively. The dose normalization facilitated data comparison among studies even when the doses differed slightly. Non-compartmental analysis was conducted for plasma and CSF $\text{hA}\beta_{40}$ data. The AUC_{∞} (area under the concentration-time curve to time infinity) was obtained by summing the area up to last sampling point based on the trapezoidal rule ($\text{AUC}_{0-\text{last}}$) and the extrapolated area under the curve obtained upon dividing the concentration of the last sample, C_{last} , by the terminal decay constant. Total body (plasma) clearance ($\text{CL}_{\text{plasma}}$) and CSF clearance (CL_{CSF}) after IV and ICV injections, respectively, were calculated as $\text{dose}_{\text{IV}}/\text{AUC}_{\infty, \text{plasma}}$ and $\text{dose}_{\text{ICV}}/\text{AUC}_{\infty, \text{CSF}}$; biliary clearance was determined as $f_{\text{bile}} \cdot \text{CL}_{\text{plasma}}$, where $f_{\text{bile}} = \text{hA}\beta_{40}$ amount in bile/ dose_{IV} .

Compartmental modeling. Compartmental models (Fig. 1) were constructed for data fitting after IV and ICV administration of $\text{hA}\beta_{40}$ with ADAPT5[®]. We employed models that embellish physiologic meanings. After extensive preliminary modeling, a three-compartment model (one central and two peripheral compartments) was considered as more consistent with data than the one or two compartment model. Fits to a one or two compartment models did not predict the data well (data not shown). To the central compartment, a brain and additional (1, 2, or 4) CSF compartments were included (Fig. 1). Model I (Fig. 1A) is the simplest model whereby the entire volume of CSF is present in the ventricles/choroid plexus/cisterna magna (CM) and subarachnoid space (SAS). Model II distinguishes the site of ICV injection (LV) from the site of CSF sampling downstream. In Model III, the 4 CSF compartments corresponds to the four ventricles, CM (sampling compartment) and subarachnoid spaces (SAS) modeled by Westerhout et al. (2012) and de Lange et al. (2017). The number of CSF compartments is based on the flow of CSF, being formed from the four ventricles at the choroid plexus then flowing from the first two lateral ventricles (LV) through the single midline third ventricle (TV) and midline fourth ventricle (FV) into the CM, then upward over the convexities of the brain in the SAS where CSF is absorbed through the arachnoid villi at

the top of the brain into the superior sagittal sinus of the venous circulation (Pardridge 2016). From the CM, CSF flows downward to the spinal cord (Fig. 1C) (Yamamoto et al. 2018).

In Models I, II and III, the intercompartmental transfer or distributional rate constants between the central, peripherals, brain, and CSF compartment are denoted as k_{12} , k_{21} , k_{13} , k_{31} , k_{14} , k_{41} , k_{45} , k_{15} , k_{51} , and k_{54} . V_1 , V_2 , V_3 , and V_4 , are the volumes of distribution for the central, two peripheral and brain compartments, respectively, and the volumes V_5 , V_6 , V_7 and V_8 are for the CSF compartments. V_4 was taken as 1.8 g (Davies and Morris, 1993). In all the models, the elimination rate constants: k_{10} , k_{40} , and k_{50} , denote the possible degradation pathways of hA β_{40} from the central, brain and CSF compartments, respectively: degradation by neprilysin in brain is denoted by k_{40} , whereas degradation in CSF occurs via the insulin degrading enzyme (k_{50}), normally considered to be an insignificant pathway (Saido and Leissring, 2012). There are four barriers: the blood brain barrier (BBB) exists between the brain capillary endothelial cells containing tight junctions, and brain parenchyma, where P-gp is present apically (k_{41}); a barrier from the ventricular ependymal cells that present as a relatively leaky barrier between the CSF and brain interstitial fluid, with k_{45} for efflux and k_{54} for the return from CSF to brain (Takasawa et al., 1997); the blood arachnoid villi barrier (BAB) lies between the fenestrated blood vessels in the meninges and the CSF in the arachnoid space, formed by tight junctions of the arachnoid epithelial cells (Yasuda et al., 2013), where return of CSF to the circulation also occurs; lastly, the blood CSF barrier (BCSFB), formed by tight junctions between the choroid plexus epithelial cells, which restrict the movement of molecules that leak from the fenestrated capillaries into the extracellular compartment of the choroid plexus, then into the CSF: k_{15} for influx from blood at the ventricular choroid plexus, and k_{51} for return to peripheral blood. For Model I where there is only one CSF compartment, k_{51} now represents the sum total of the return from BCSFB, BAB and CSF bulk flow. For Model II, k_{51} represents the return from the BCSFB, and k_{61} , the return CSF flow and efflux functionality at the arachnoid villi (BAB). For Model III, k_{51} represents the return from the BCSFB with k_{81} representing the return CSF flow and efflux functionality at the BAB.

Fitting. The ADAPT5[®] System Analysis Software (Biomedical Simulations Resource, Version 5.0.53; University of Southern California, Los Angeles, CA) was used for data fitting with the Maximum-Likelihood Expectation Maximization (MLEM) algorithm. Initial estimates were determined from curve stripping analysis. Simultaneously fitting of both the control and calcitriol data sets was not successful. First, only first-order conditions are assumed to prevail. The first fit was based on the combined control data of hA β ₄₀ in plasma and CSF after IV and ICV injections into the rat. The second fit was performed on model fitting to the combined data from IV and ICV injections to the treated rats. Preliminary fitting showed that inclusion of the rate constant k_{15} in Model I did not affect the fit, as the value was very low and could be omitted. The same was observed for k_{51} . For subsequent fits to Model II and III, setting k_{15} or $k_{51}=0$ did not affect the fit (Supplemental Tables 1 and 2), suggesting that the net transport at the BCSFB is insignificant. The decision agrees with reports on the low permeability of unconjugated human A β in the rat (Saito et al., 1995; Poduslo et al., 1999; Kandimalla et al., 2005), and that the activity at the BCSFB is much lower (1/30) than that at the BBB (Morris et al., 2017).

As a starting point, Model I (Fig. 1A) was used to fit the hA β ₄₀ IV and ICV data sets in absence of calcitriol treatment. The fit provided both individual and population best fits of the data to render final estimates. These rate constants were then used as initial estimates to fit the IV and ICV sets of data with calcitriol treatment in the second fit. Since preliminary modeling showed that volume of the CSF compartment (V_5) was increased 5-fold after calcitriol treatment without any compelling physiological reasons, the volume estimates of $V_{1,plasma}$ and $V_{5,CSF}$ from the first fit (control data set) were fixed for the second fit (calcitriol treatment data, labeled as the model “A”); in other fits (model “B”), we also fixed the CSF return rate constant, k_{51} , k_{61} , or k_{81} . We also assigned physiological volumes for fitting (Davies and Morris, 1993) for Model II. For best fits, graphs were visualized (prediction plots), and statistical outputs, the weighted sum of squared residuals (WSSR) and Akaike Information Criterion (AIC); the lowest number suggest the best fit. We examined the F -test statistic (with use of degrees of freedom and

WSSR to calculate the F -score for comparison to the critical F -value, with the significance level, α , as 0.05) for the best fit (Boxenbaum et al., 1974).

Western Immunoblotting. Rat hemibrains were homogenized in 5x homogenizing buffer containing protease inhibitors (1:100; v/v), and the brain homogenate was subsequently centrifuged at 3,000x g for 10 min at 4 °C (Chow et al., 2011). The resulting brain supernatant was further diluted with homogenizing buffer and centrifuged at 33,000 x g for 60 min at 4 °C. The resultant pellet or non-nuclear crude membrane fraction was resuspended in 200-300 μ L of resuspension buffer containing protease inhibitor (1:100; v/v) (Chow et al., 2011), and protein concentration was determined by the Lowry method (1951). Aliquots containing 40 μ g of non-nuclear (crude) membrane protein in brain for P-gp, neprilysin, and Mrp1 (multi-drug resistance associated protein 1) and 5 μ g for Lrp1 (low-density lipoprotein receptor-related protein 1), were resolved with 10% SDS-polyacrylamide gel electrophoresis. The resolved proteins were wet transferred (BioRad, Mississauga, ON) onto nitrocellulose membranes (GE Health, Mississauga, ON) and blocked with 5% skim milk dissolved in Tris-buffered saline + 0.1% Tween-20 (1X TBS-T) at room temperature for 1 h. After this step, blots were washed once with TBS-T solution, cut, and probed over night at 4°C with respective primary anti-P-gp (1:500; v/v), anti-neprilysin (1:1000; v/v), anti-Mrp1 (1:50; v/v), anti-Lrp1 (1:50,000; v/v), and anti-Gapdh (1:15,000; v/v) antibodies in 2% skim milk TBS-T solution. The blots were washed 3 times with TBS-T (15 min for each wash) and incubated further at room temperature for 2 h with goat anti-mouse or rabbit IgG secondary antibody conjugated to horseradish peroxidase (1:1,000 for P-gp, neprilysin, Mrp1, Lrp1, and 1:10,000 for Gapdh; v/v) in 2% skim milk TBS-T solution. After 2 h of incubation, blots were washed again 3 times with TBS-T (15 min for each wash) and imaged by the enhanced chemiluminescence reagent (Amersham, GE Health) with ChemiDoc MP (BioRad). The band intensities were quantified by densitometry and normalized to the house keeping protein, Gapdh.

Statistical analysis. All concentration data were normalized to dose and expressed as %dose·mL⁻¹, and data are expressed as mean ± SD. The Student's unpaired *t*-test was conducted for the comparison of Western Immunoblots and parameters obtained for untreated and corn oil treated rats by non-compartmental analysis, and the Wilcoxon Rank Sum test (nonparametric test, R) was conducted for individual parameters from population data set, and the significant *P* value was < 0.05.

Results

Quantitation of hA β ₄₀

Calibration curves that were generated from different types of media (SDB, 10-10,000-fold diluted plasma, 5-fold diluted plasma by mixing 10 μ L plasma with 40 μ L SDB or 50 μ L undiluted plasma, or aCSF) were used for appraisal of the matrix effect. The limit of quantitation was 7.81 pg·mL⁻¹ for plasma and CSF hA β ₄₀ concentrations. Clearly, the matrix effect that resulted in quenching of absorbance by plasma components was observed among the 1,000 to 8,000 pg·mL⁻¹ samples (Fig. 2A); the greater the % rat plasma, the greater the magnitude of quenching. Signal suppression by the undiluted plasma was about 50% for the 8,000 pg·mL⁻¹ sample. The calibration curves prepared in SDB and 5-fold diluted plasma were essentially identical, whereas values of the standards generated in 50 μ L undiluted plasma were lower (Fig. 2B). The calibration curves prepared in SDB and 5-fold diluted plasma were essentially identical, whereas values of standards generated in 50 μ L undiluted plasma were diminished (Fig. 2B). For standards prepared in aCSF, the assayed value for the highest calibration standard was higher than that prepared in SDB or the 10- to 10,000-fold diluted plasma, but values for other calibration standards were all similar (Fig. 2B). Hence, multiple calibration curves were prepared in different matrices and different dilutions of the sample (Fig. 2B). Since most of the measured concentrations were between 7.81 to 250 pg·mL⁻¹, the resulting concentrations after interpolation were similar for the samples prepared in SDB or in plasma samples with sufficiently high dilution (>10-10,000-fold dilution with SDB). The calibration curve prepared in SDB was deemed appropriate for the determination of hA β ₄₀ samples at earlier time points (>10 to 10,000-fold dilution), whereas for the late-in-time undiluted plasma samples (last data point at 180 min), the calibration curve that was prepared in undiluted rat plasma was used for quantitation.

Pharmacokinetics of hA β ₄₀

Non-compartmental modeling of IV data in untreated versus corn oil treated rats. We first tested whether corn oil, the vehicle for calcitriol administration, affected the kinetics of hA β ₄₀ in groups of rats. In both groups of rats given IV hA β ₄₀, similar multi-exponential decay profiles were observed for the hA β ₄₀ in plasma; CSF concentrations rose quickly and remained quite constant over the 180 min of sampling (Fig. 3A). The apparent terminal $t_{1/2}$ s of hA β ₄₀, estimated by regression of the log-linear portions of the plasma decay curves, were similar (24.5 ± 0.05 min and 16.8 ± 5.66 min for the untreated and the corn oil-treated rats (Fig. 3B), respectively; $P > 0.05$), whereas those for CSF were considerably longer (75.5 ± 17.9 min and 47.9 ± 20.9 min, respectively; $P > 0.05$). The $AUC_{\infty, \text{plasma}}$ (extrapolated to infinity) normalized to the dose for the injections in saline and corn oil (vehicle) pretreated rats were not different ($P > 0.05$; Table 1), yielding similar plasma clearances (CL_{plasma}) of 17.9 ± 6.20 and 23.2 ± 2.21 mL·min⁻¹·kg⁻¹ for both groups. The total amounts recovered in bile, collected for untreated rats, and the fraction of dose (f_{bile}) excreted into bile were both very low, and hA β ₄₀ was undetectable in urine. The partition coefficient for CSF/plasma ($K_{p, \text{CSF:plasma}}$), calculated as ratio of $AUC_{\infty, \text{CSF}}/AUC_{\infty, \text{plasma}}$, was low and similar (0.0085 ± 0.00211 and 0.0099 ± 0.00680 , $P > 0.05$) between the untreated and corn oil treated rats. The composite data showed that corn oil did not interfere with the kinetics of hA β ₄₀ (Table 1).

Compartmental modeling and fitting of data after IV and ICV injections. Because the hA β ₄₀ concentration-time profiles of the control rats, with or without corn oil treatment, were similar after IV hA β ₄₀ dosing, data for this first group of rats were combined and consolidated as the control IV group ($n = 16$). These IV data that exhibited the shorter $t_{1/2}$ s in plasma were for comparison to the control data after ICV injections ($n=4$), which showed that hA β ₄₀ plasma and CSF concentrations decayed in unison. All models (Fig. 1) were used for fitting of the IV and ICV data for the control groups (fit 1), then for the IV and ICV data for the treatment groups (fit 2). Preliminary fits showed minor and 5-fold changes in $V_{1, \text{plasma}}$ and $V_{5, \text{CSF}}$, respectively, for Model I. Because there is no physiological basis of these volume changes, we

constrained these parameters and assigned the fitted estimates from the first fit as volumes of plasma and CSF for the second fit (“A” versions of models); another added constraint was carried out by setting the return CSF clearance: $k_{51} \cdot V_{5,CSF}$, $k_{61} \cdot V_{6,CSF}$ and $k_{81} \cdot V_{8,CSF}$ for Models I, II, and III, respectively (“B” versions of the models). The F scores for all models were not significantly different from Model I for all fits, although differences in WSSR and AIC were noted (Table 2). The key changes of the derived rate constants from Models I, IA and IB (Table 3), and Models II, IIA, IIB, III, IIIA, and IIIB (Supplemental Tables 1 and 2; Supplemental Figs. 1 and 2) are summarized. Statistically, best fits were observed for Model I and IA (Fig. 4), and $V_{5,CSF}$, whether being constraint or not, is not important. Then Model II which revealed low WSSR and AIC values (Table 2) and excellent prediction plots (Supplemental Fig. 1) was also found to be satisfactory, but Model II fits were associated with higher CVs (Supplemental Table 1). Fits for Models IB, IIA, IIB, and all Model III (Fig. 4 & Supplemental Figs. 1 and 2) and other models (data not shown) were poorer. For the treatment data, the ICV CSF data for Models IIB and IIC were consistently over-predicted, whereas the ICV plasma data for Models IB and III were consistently under-predicted (Fig. 4 & Supplemental Figs. 1 and 2). Additionally, more complex models, including addition of an interstitial fluid (ISF) or glymphatic compartment or a semi-PBPK model, did not improve the fit to our data (data not shown). The data for the non-treatment and treatment groups were within the predicted 5% and 95% confidence interval (shaded area between dotted red or blue lines) for Model I (Fig. 5).

For Model I, k_{41} , k_{45} and k_{51} were increased 1.8- 3.4- and 5.4-fold, respectively; $V_{5,CSF}$ was increased 5.3-fold ($P < .05$) after calcitriol treatment. This volume change was found to be unimportant since Model IA (assigning $V_{5,CSF}$ and $V_{1,plasma}$ as constants) also predicted the data well (Fig. 4). Upon restraining the volumes of plasma and CSF (Model IA), k_{41} , k_{45} and k_{51} were increased 1.7-, 1.6- and 8.2-fold, respectively. The increase in k_{51} could be explained when P-gp, present abundantly at the arachnoid villi (BAB) (Yasuda et al., 2013), is also induced by calcitriol. Upon further restraining k_{51} , $V_{1,plasma}$, and $V_{5,CSF}$ as constants (Model IB), k_{41} and k_{45} were increased 1.25- and 2.75-fold, respectively. In all fits, the CSF ($k_{50} \cdot V_{5,CSF}$) and brain ($k_{40} \cdot V_{4,brain}$) degradation clearances were unchanged with calcitriol treatment (Table

3). A closer look at the calcitriol-treated group revealed a slightly but insignificantly faster terminal phase when compared to the control group. The CL_{plasma} ($k_{10} \cdot V_{1,\text{plasma}}$) was increased significantly only for Model I from 21.8 to 25.8 $\text{mLmin}^{-1}\text{kg}^{-1}$ with calcitriol-treatment and not for Model IA nor Model IB (Table 3). For Model II, the fitted values of most of the constants were unchanged, but high CVs were observed. For Model III where there is underprediction of CSF data, there were minor changes in the CSF flow rate constants, k_{67} and k_{78} , and k_{50} , which increased with calcitriol treatment. CL_{plasma} for Model II was double that of Model I for control data, and treatment increased the value from 44.5 to 55.9 $\text{mLmin}^{-1}\text{kg}^{-1}$ insignificantly (Supplemental Table 1), whereas CL_{plasma} for Model III was similar to that of Model I and the value remained unchanged with calcitriol treatment (Supplemental Table 2). Overall, Model I is best, but Models I and II fail to explain the ratio, $k_{41}/k_{45} < 1$, which is inconsistent with known abundances of P-gp in the BBB (Qosa et al., 2014; Morris et al., 2017); only Model III has the correct pattern.

Commonality of the models. Generally speaking, there is faster equilibration between the central and peripheral compartments than with the brain compartment (k_{14}) for all of the models (see Tables 1 and Supplemental Tables 1 to 2). The transfer rate constant from plasma to brain (k_{14}) is slow among the distributional rate constants; k_{15} is even slower and the fit was not altered when its value was set to zero; the efflux rate constants at the BBB (k_{41}) and ventricular barrier (k_{45}) are faster than the influx constants from plasma, k_{14} and k_{15} . All of the brain/CSF distributional rate constants (k_{14} , k_{41} , k_{45} , k_{51} , and k_{54}) are much slower than k_{12} , k_{13} , k_{21} and k_{31} , the distributional rate constants between plasma and the peripheral compartments 1 and 2.

Modeling and Simulations. To further understand the pharmacokinetics of $\text{hA}\beta_{40}$, simulations were performed based on the fitted parameters of the best model, Model I. The amount of $\text{hA}\beta_{40}$ in brain (expressed as %dose) was normalized to the brain volume (1.8 g) (Davies and Morris, 1993). Plasma concentrations were shown to decay more rapidly with a shorter plasma $t_{1/2}$ following IV versus ICV injection, but then plasma levels tapered off and levels became parallel to those for the brain and CSF

(Fig. 6). This is due to the rapid distribution of hA β ₄₀ (k_{12} and k_{13}) to the peripheral compartments and very slow permeation (k_{14} and $k_{15} \sim 0$) into the brain and CSF. The return of hA β ₄₀ from brain and CSF (k_{41} and k_{51}) to the circulation were also slower than k_{21} and k_{31} (Tables 1 and Supplemental Tables 1 and 2), and with time, the terminal $t_{1/2}$ s of the plasma, brain, and CSF for hA β ₄₀ all became similar (Fig. 6). The slow distribution rate constants k_{41} and k_{51} relative to the faster k_{21} and k_{31} rate constants rate-limit the distribution of hA β ₄₀ from brain/CSF back to plasma, resulting in an apparently faster plasma $t_{1/2}$ after IV administration. For ICV administration, CSF and brain levels are closer to the injection site, and the CSF $t_{1/2}$ paralleled that in plasma.

The simulated AUC_{∞} s for Model I further revealed other dispositional patterns of the administration route and induction by calcitriol (Table 4). The route of the injection results in higher AUC_{∞} for the injected site, for example, plasma exposure ($AUC_{\infty, \text{plasma}, \text{IV}}$) after IV administration is higher than after ICV, and the pattern persists with absence or presence of calcitriol treatment (Fig. 6, Tables 3 and 4). Similarly, CSF exposure ($AUC_{\infty, \text{CSF}, \text{ICV}}$) is much higher after ICV than IV administration, and the pattern also persists with or without calcitriol treatment. There is little change in $AUC_{\infty, \text{brain}}$ after IV or ICV administration, or calcitriol treatment, suggesting that this parameter is relatively insensitive to calcitriol-mediated changes in brain hA β ₄₀ disposition (Table 3). The $AUC_{\infty, \text{plasma}, \text{IV}}$ is much higher than $AUC_{\infty, \text{brain}, \text{IV}}$ and $AUC_{\infty, \text{CSF}, \text{IV}}$ after IV administration due to the slow distribution of hA β ₄₀ into brain and CSF (Table 4). The $AUC_{\infty, \text{CSF}, \text{ICV}}$ is similar to $AUC_{\infty, \text{brain}, \text{ICV}}$, and these greatly exceed $AUC_{\infty, \text{plasma}, \text{ICV}}$ after ICV administration, reflecting slow efflux of k_{41} and k_{51} at the BBB and BCSFB/BAB (Table 3). Overall, calcitriol treatment resulted in a substantial reduction of $AUC_{\infty, \text{plasma}, \text{IV}}$ and $AUC_{\infty, \text{CSF}, \text{IV}}$ after IV administration according to Model I, and there is decreased $AUC_{\infty, \text{CSF}, \text{ICV}}$ but increased $AUC_{\infty, \text{plasma}, \text{ICV}}$ after ICV administration due to the increases in k_{41} (BBB), k_{45} and k_{51} (Table 4).

Western Immunoblot for efflux and degradation proteins

P-gp, neprilysin, Lrp1, and Mrp1 relative protein expressions. Western immunoblotting was conducted to determine relative protein changes in brain P-gp and Mrp1, neprilysin, and Lrp1 for efflux transporters

and degradation enzyme(s) in the crude brain non-nuclear membrane fraction. Samples from the corn oil treated controls (hA β_{40} IV) were compared to the calcitriol-treated rats (IV and ICV hA β_{40}). Calcitriol treatment resulted in a significant increase (~ 2 -fold) in P-gp protein expression in the rat brain, an observation similar to that observed in mouse (Chow et al., 2011) and rat (Durk et al., 2015), and agreed with the predictions of Models I and IA (1.79- and 1.72- increase in k_{41}). However, neprilysin, Lrp1, and Mrp1 relative protein expression levels were unchanged with calcitriol treatment (Fig. 7). Levels of Bcrp protein expression were also not altered, as we found previously (Durk et al., 2012). The lack of change neprilyin protein agreed with the lack of change in the degradation rate constant (k_{40}) in the brain.

Discussion

Being assured that our strategy of using multiple calibration curves circumvented the sample matrix interference problem in the ELISA assay (Fig. 2), we proceeded to define the pharmacokinetics of hA β ₄₀. After IV injection, a low biliary clearance ($0.00161 \pm 0.00124 \text{ mL} \cdot \text{min}^{-1} \cdot \text{kg}^{-1}$) and even lower (undetectable) renal clearance were noted for hA β ₄₀. The apparent plasma $t_{1/2}$ and IV plasma clearance were 24.5 min and 18 to 22 $\text{mL} \cdot \text{min}^{-1} \cdot \text{kg}^{-1}$, respectively (Table 1), observations that are compatible with those in mice ($t_{1/2} = 25.5 \text{ min}$) (Shibata et al., 2000) and rats (Saito et al., 1995) where the $t_{1/2}$ was 27 min and V_{ss} was $273 \pm 59 \text{ mL} \cdot \text{kg}^{-1}$. Kandimalla et al. (2005; 2006) reported faster I¹²⁵-A β ₄₀ half-lives of 9.2 ± 2.3 and $11.2 \pm 5.1 \text{ min}$ after IV administration and longer half-lives of 30 and 50 min in a later study (Kandimalla et al., 2007). CL_{plasma} was $10.1 \pm 1.2 \text{ mL} \cdot \text{min}^{-1} \cdot \text{kg}^{-1}$ (Kandimalla et al., 2005; 2006) after IV administration of the radioactively labeled peptide, and 5.48 ± 0.38 and $4.58 \pm 0.57 \text{ mL} \cdot \text{min}^{-1} \cdot \text{kg}^{-1}$, respectively, in two- and twenty-five-month-old mice, respectively (Nishida et al., 2009). These smaller clearance values are likely due to radiolabeled metabolites present that contributed to a higher area under the curve. Our data suggest that IV injected hA β ₄₀ crosses from plasma into the brain and CSF slowly and that hA β ₄₀, when injected into the rat CSF after ICV injection is detected in the systemic circulation, as found by others (Gherssi-Egea et al., 1996b; Spies et al., 2012; Tarasoff-Conway et al., 2015), suggesting that hA β ₄₀ is able to traverse from the CSF to plasma, either via the BCSFB, CSF flow, or arachnoid barrier (Fig. 3). A notable observation is the faster $t_{1/2}$ for plasma but a slightly longer $t_{1/2}$ for CSF (76 min) within 180 min in our IV studies (Fig. 3). The lower concentrations of hA β ₄₀ in CSF after IV dosing agree with other studies, showing that A β permeability from plasma into brain (via BBB) or CSF (via k_{15} , BCSFB) is poor (Saito et al., 1995; Poduslo et al., 1999; Kandimalla et al., 2005). Interestingly, reports on intracerebral administration of I¹²⁵-A β ₄₀ concluded that the major clearance pathways are via the BBB or degradation while efflux across BCSFB via bulk transport is diminutive (Shiiki et al., 2004; Yamada et al., 2008; Qosa et al., 2014), and that I¹²⁵-A β ₄₀ administered into CSF via ICV poorly diffuses into brain

tissue but is quickly cleared from CSF to blood (same for ^{125}I -BDNF and ^{14}C -sucrose) (Yan et al., 1994; Ghersi-Egea et al., 1996a; 1996b).

We modeled the IV and ICV data based on Models I, II, and III, and variations thereof. In Model I (Fig. 1A), the brain compartment is associated with intercompartmental rates constants, k_{14} and k_{41} , at the BBB, and k_{15} and k_{51} at the BCSFB/choroid plexus, although the return clearance of $V_{5,\text{CSF}}$ k_{51} , denotes return from the ventricular CSF (BCSFB), CSF bulk flow and P-gp efflux at the arachnoid villi (BAB) to the central compartment. Modification of Model I with more CSF compartments provided more physiological relevance but did not improve the fits (Fig. 1). The F scores showed that fixing the volumes (version “A”) or the CSF return clearance terms ($V_{5,\text{CSF}} \cdot k_{51}$, $V_{6,\text{CSF}} \cdot k_{61}$ or $V_{8,\text{CSF}} \cdot k_{81}$) (version “B”) or assignment of physiological volumes (Davies and Morris, 1993; Yamamoto et al., 2018) did not significantly alter the F score (Table 2). This is because of the models, being catenary in nature with interconnections between brain and CSF with plasma, and the brain with CSF, rendered more uncertainty/ambiguity. Therefore, we used the prediction plots (Fig. 4 and Supplemental Figs. 1 and 2) and established Models I and IA as the best models. Model I predicts that P-gp efflux at the BBB (k_{41}) and BAB (k_{51}) is increased by calcitriol treatment. The trend for the 2-fold increase in P-gp protein expression in brain (Fig. 7) is in agreement with Model I predictions (Table 3). The influx of $\text{hA}\beta_{40}$ by P-gp into the CSF at the choroid plexus (k_{15}) is unimportant, since inclusion or deletion of k_{15} did not alter the fit. However, the model also predicts that calcitriol treatment results in a 3.4-fold increase in k_{45} , the rate constant for transfer of $\text{hA}\beta_{40}$ from brain into CSF via the leaky ependymal cells in the ventricles. Model II, although with high CV in the fits, is also acceptable. Model III fits are poor.

Although P-gp protein expression is predominantly expressed apically at the BBB, there is controversy over the localization of P-gp at the BCSFB. Rao et al. (1999) demonstrated the presence of P-gp apically in primary culture of the choroid plexus epithelial cells from 1-week old neonatal rat’s lateral and fourth ventricles, but others failed to detect P-gp apically at the choroid plexus among rats of different ages (Gazzin et al., 2008; Roberts et al., 2008, Pascale et al., 2011; Yasuda et al., 2013). According to

brain anatomy, the choroid plexus is only a portion of the BCSFB. The arachnoid epithelium (arachnoid mater) lining the subarachnoid space where the CSF fills (above the pia mater) constitutes another barrier (Yasuda et al., 2013) and the cranial and spinal arachnoid villi constitute the predominant site of CSF clearance into the venous outflow system (Sakka et al., 2011). Especially when the efflux from BCSFB is slow, the sum of this efflux and CSF flow and efflux of the BAB constitute the return clearance from CSF to the blood compartment, $(k_{51} \cdot V_{5,CSF})$, which was increased 5.4-fold according to Model I (Table 3). It should be noted that other clearance processes also exist, such as degradation processes by microglia and other enzymes (insulin degradation enzyme, angiotensin and or endothelin converting enzyme) (Saido and Leissring, 2012).

With Model I being the best and simplest model, the disparity in the $t_{1/2s}$ was explained with simulations based on the slow distribution constants, k_{14} , k_{15} , k_{41} and k_{51} , between plasma and brain/CSF in comparison to the faster constants (k_{12} , k_{13} , k_{21} and k_{31}) between plasma and peripheral compartments (Table 3 and Supplemental Tables 1 to 2). The difference in $t_{1/2s}$ between plasma and CSF within the 180 min observation period after IV injection disappeared at around 600 min, revealing the slower terminal γ phase of about 50-60 min in plasma that paralleled the $t_{1/2s}$ in CSF and brain following IV dosing (Fig. 6). Due to the slow transfer rate constant to brain (k_{14}) or CSF ($k_{15} = 0$) as rate-limiting steps after IV dosing and k_{41} and k_{51} after ICV dosing, we noted that the K_p values are different due to differences in $AUC_{\infty s}$ in the plasma and CSF (based on simulations) and their dependence on the route of administration (Table 4). We also showed that the specific site of injection of $hA\beta_{40}$ may lead to preferential routes of clearance by the brain, as shown by others (Shiiki et al., 2004; Yamada et al., 2008; Qosa et al., 2014), whether $hA\beta_{40}$ is effluxed across BBB or undergoes brain enzymatic degradation. Substrates administered into brain tissue by intracerebral injections are preferentially cleared via the BBB, whereas substrates given by intracerebroventricular (ICV) injections into the CSF are preferentially cleared via the BCSFB/BAB and CSF bulk flow. $hA\beta_{40}$ distribution into the CSF is not a measure of BBB permeability but is a measure of

transport across the choroid plexus (k_{15}) as well as the arachnoid barrier (k_{51}), and k_{45} , efflux at the ventricular barrier. The CSF is not a homogeneous space in brain parenchyma, and a substrate injected into CSF will distribute in a pattern stepwise along the ventricles to perfuse brain tissue at the arachnoid villi and ependymal surface of brain or spinal cord, then return to blood.

To conclude, it was shown that matrix interference in the ELISA method was circumvented by appropriate calibration curves prepared in sample matrix. After verification that corn oil did not affect $\text{hA}\beta_{40}$ kinetics or concentration-time profile, we established that Model I best fit the data from IV and ICV injections in both untreated and calcitriol-treated rats. Calcitriol treatment altered $\text{hA}\beta_{40}$ disposition via the induction of P-gp, increasing efflux at the BBB (increase in k_{41}) and maybe the BAB (increase in k_{51}). Although calcitriol treatment induced P-gp protein expression by 2-fold, other clearance mechanisms may exist, particularly at the arachnoid villi barrier. The model predicts a slow equilibration between plasma and CSF due to slow permeation of $\text{hA}\beta_{40}$ to the brain and CSF, but when data were simulated over a long period of time, the $t_{1/2s}$ and levels of $\text{hA}\beta_{40}$ in plasma, CSF and brain all decayed in unison. Under this circumstance, the plasma $\text{hA}\beta_{40}$ profile would better reflect that in the brain. Hence, use of plasma $\text{hA}\beta_{40}$ as a biomarker by itself or as a ratio with $\text{hA}\beta_{42}$ to reflect brain concentrations or AD progression must proceed with caution.

Acknowledgements

We thank our collaborator, InterVivo Solutions Inc., for sharing use their facility and their contribution to the experiments.

Authorship Contributions

Participated in research design: H.B. Peng, I.A.M. de Lannoy, and K.S. Pang.

Conducted animal experiments: H.B. Peng, K. Noh, V. Saldivia, S. Serson, and A. Toscan.

Conducted experiments: H.B. Peng and S. Pan.

Performed data fitting: H.B. Peng, K. Noh, and K.S. Pang.

Wrote or contributed to the writing of the manuscript: H.B. Peng, I.A.M. de Lannoy, and K.S. Pang.

Conflicts

The authors declare no conflicts.

References

- Abramowski D, Wiederhold KH, Furrer U, Jatton AL, Neuenschwander A, Runser MJ, Danner S, Reichwald J, Ammaturo D, Staab D, Stoeckli M, Rueeger H, Neumann U, and Staufenbiel M (2008) Dynamics of Abeta turnover and deposition in different beta-amyloid precursor protein transgenic mouse models following gamma-secretase inhibition. *J Pharmacol Exp Ther* **327**:411-424.
- Alemi M, Gaiteiro C, Ribeiro CA, Santos LM, Gomes JR, Oliveira SM, Couraud PO, Weksler B, Romero I, Saraiva MJ, and Cardoso I (2016) Transthyretin participates in beta-amyloid transport from the brain to the liver--involvement of the low-density lipoprotein receptor-related protein 1? *Sci Rep* **6**:20164.
- Bateman RJ, Munsell LY, Morris JC, Swarm R, Yarasheski KE, and Holtzman DM (2006) Human amyloid-beta synthesis and clearance rates as measured in cerebrospinal fluid *in vivo*. *Nat Med* **12**:856-861.
- Bates KA, Verdile G, Li QX, Ames D, Hudson P, Masters CL, and Martins RN (2009) Clearance mechanisms of Alzheimer's amyloid-beta peptide: implications for therapeutic design and diagnostic tests. *Mol Psychiatry* **14**:469-486.
- Bell RD, Sagare AP, Friedman AE, Bedi GS, Holtzman DM, Deane R, and Zlokovic BV (2007) Transport pathways for clearance of human Alzheimer's amyloid beta-peptide and apolipoproteins E and J in the mouse central nervous system. *J Cereb Blood Flow Metab* **27**:909-918.
- Biere AL, Ostaszewski B, Stimson ER, Hyman BT, Maggio JE, and Selkoe DJ (1996) Amyloid beta-peptide is transported on lipoproteins and albumin in human plasma. *J Biol Chem* **271**:32916-32922.
- Boxenbaum HG, Riegelman S, and Elashoff RM (1974) Statistical estimations in pharmacokinetics. *J Pharmacokin Biopharm* **2**:123-146.

- Chow EC, Durk MR, Cummins CL and Pang KS (2011) $1\alpha,25$ -Dihydroxyvitamin D₃ upregulates P-glycoprotein activities via the vitamin D receptor and not farnesoid X receptor in both *fxr*(-/-) and *fxr*(+/+) mice, and increased renal and brain efflux of digoxin in mice *in vivo*. *J Pharmacol Exp Ther* **337**:846-859.
- Cirrito JR, May PC, O'Dell MA, Taylor JW, Parsadanian M, Cramer JW, Audia JE, Nissen JS, Bales KR, Paul SM, DeMattos RB, and Holtzman DM (2003) *In vivo* assessment of brain interstitial fluid with microdialysis reveals plaque-associated changes in amyloid-beta metabolism and half-life. *J Neurosci* **23**:8844-8853.
- Davies B and Morris T (1993) Physiological parameters in laboratory animals and humans. *Pharm Res* **10**:1093-1095.
- Deane R, Bell RD, Sagare A, and Zlokovic BV (2009) Clearance of amyloid-beta peptide across the blood-brain barrier: implication for therapies in Alzheimer's disease. *CNS Neurol Disord Drug Targets* **8**:16-30.
- de Lange ECM, van den Brink W, Yamamoto Y, de Witte WEA, and Wong YC (2017) Novel CNS drug discovery and development approach: model-based integration to predict neuro-pharmacokinetics and pharmacodynamics. *Expert Opin Drug Discov* **12**:1207-1218.
- Durk MR, Han K, Chow EC, Ahrens R, Henderson JT, Fraser PE, and Pang KS (2014) $1\alpha,25$ -Dihydroxyvitamin D₃ reduces cerebral amyloid-beta accumulation and improves cognition in mouse models of Alzheimer's disease. *J Neurosci* **34**:7091-7101.
- Durk MR, Chan GN, Campos CR, Peart JC, Chow EC, Lee E, Cannon RE, Bendayan R, Miller DS, Pang KS (2012) $1\alpha,25$ -Dihydroxyvitamin D₃-liganded vitamin D receptor increases expression and transport activity of P-glycoprotein in isolated rat brain capillaries and human and rat brain microvessel endothelial cells. *J Neurochem* **123**:944-53.

- Durk MR, Fan J, Sun H, Yang Y, Pang H, Pang KS, and de Lannoy IA (2015) Vitamin D receptor activation induces P-glycoprotein and increases brain efflux of quinidine: an intracerebral microdialysis study in conscious rats. *Pharm Res* **32**:1128-1140.
- Gazzin S, Strazielle N, Schmitt C, Fevre-Montange M, Ostrow JD, Tiribelli C, and Gherzi-Egea JF (2008) Differential expression of the multidrug resistance-related proteins ABCb1 and ABCc1 between blood-brain interfaces. *J Comp Neurol* **510**:497-507.
- Gherzi-Egea JF, Finnegan W, Chen JL, and Fenstermacher JD (1996a) Rapid distribution of intraventricularly administered sucrose into cerebrospinal fluid cisterns via subarachnoid velae in rat. *Neuroscience* **75**:1271-1288.
- Gherzi-Egea JF, Gorevic PD, Ghiso J, Frangione B, Patlak CS, and Fenstermacher JD (1996b) Fate of cerebrospinal fluid-borne amyloid beta-peptide: rapid clearance into blood and appreciable accumulation by cerebral arteries. *J Neurochem* **67**:880-883.
- Ghiso J, Shayo M, Calero M, Ng D, Tomidokoro Y, Gandy S, Rostagno A, and Frangione B (2004) Systemic catabolism of Alzheimer's Abeta40 and Abeta42. *J Biol Chem* **279**:45897-45908.
- Hansen DV, Hanson JE, and Sheng M (2018) Microglia in Alzheimer's disease. *J Cell Biol* **217**:459-472.
- Hardy JA and Higgins GA (1992) Alzheimer's disease: the amyloid cascade hypothesis. *Science* **256**:184-185.
- Hartmann T, Bieger SC, Brühl B, Tienari PJ, Ida N, Allsop D, Roberts GW, Masters CL, Dotti CG, Unsicker K, and Beyreuther K (1997) Distinct sites of intracellular production for Alzheimer's disease A beta40/42 amyloid peptides. *Nat Med* **3**:1016-1020.
- Haass C, Koo EH, Mellon A, Hung AY and Selkoe DJ (1992) Targeting of cell-surface beta-amyloid precursor protein to lysosomes: alternative processing into amyloid-bearing fragments. *Nature* **357**:500-503.
- Hofrichter J, Krohn M, Schumacher T, Lange C, Feistel B, Walbroel B, Heinze HJ, Crockett S, Sharbel TF, and Pahnke J (2013) Reduced Alzheimer's disease pathology by St. John's Wort treatment is

independent of hyperforin and facilitated by ABCC1 and microglia activation in mice. *Curr Alzheimer Res* **10**:1057-1069.

Iwata N, Higuchi M, and Saido TC (2005) Metabolism of amyloid-beta peptide and Alzheimer's disease. *Pharmacol Ther* **108**:129-148.

Iwata N, Tsubuki S, Takaki Y, Watanabe K, Sekiguchi M, Hosoki E, Kawashima-Morishima M, Lee HJ, Hama E, Sekine-Aizawa Y, and Saido TC (2000) Identification of the major Abeta1-42-degrading catabolic pathway in brain parenchyma: suppression leads to biochemical and pathological deposition. *Nat Med* **6**:143-150.

Jan A, Hartley DM, and Lashuel HA (2010) Preparation and characterization of toxic Abeta aggregates for structural and functional studies in Alzheimer's disease research. *Nat Protoc* **5**:1186-1209.

Juranek JK, Daffu GK, Geddis MS, Li H, Rosario R, Kaplan BJ, Kelly L, and Schmidt AM (2016) Soluble RAGE treatment delays progression of amyotrophic lateral sclerosis in SOD1 mice. *Front Cell Neurosci* **10**:117.

Kandimalla KK, Curran GL, Holasek SS, Gilles EJ, Wengenack TM, and Poduslo JF (2005) Pharmacokinetic analysis of the blood-brain barrier transport of ¹²⁵I-amyloid beta protein 40 in wild-type and Alzheimer's disease transgenic mice (APP,PS1) and its implications for amyloid plaque formation. *J Pharmacol Exp Ther* **313**:1370-1378.

Kandimalla KK, Curran GL, Holasek SS, Gilles EJ, Wengenack TM, Ramirez-Alvarado M, and Poduslo JF (2006) Physiological and biophysical factors that influence Alzheimer's disease amyloid plaque targeting of native and putrescine modified human amyloid beta40. *J Pharmacol Exp Ther* **318**:17-25.

Kandimalla KK, Wengenack TM, Curran GL, Gilles EJ, and Poduslo JF (2007) Pharmacokinetics and amyloid plaque targeting ability of a novel peptide-based magnetic resonance contrast agent in wild-type and Alzheimer's disease transgenic mice. *J Pharmacol Exp Ther* **322**:541-549.

- Krohn M, Lange C, Hofrichter J, Scheffler K, Stenzel J, Steffen J, Schumacher T, Bruning T, Plath AS, Alfen F, Schmidt A, Winter F, Rateitschak K, Wree A, Gsponer J, Walker LC, and Pahnke J (2011) Cerebral amyloid-beta proteostasis is regulated by the membrane transport protein ABCC1 in mice. *J Clin Invest* **121**:3924-3931.
- Kuo YM, Emmerling MR, Lampert HC, Hempelman SR, Kokjohn TA, Woods AS, Cotter RJ, and Roher AE (1999) High levels of circulating Abeta42 are sequestered by plasma proteins in Alzheimer's disease. *Biochem Biophys Res Commun* **257**:787-791.
- Lam FC, Liu R, Lu P, Shapiro AB, Renoir JM, Sharom FJ, and Reiner PB (2001) beta-Amyloid efflux mediated by p-glycoprotein. *J Neurochem* **76**:1121-1128.
- Lanz TA and Schachter JB (2006) Demonstration of a common artifact in immunosorbent assays of brain extracts: development of a solid-phase extraction protocol to enable measurement of amyloid-beta from wild-type rodent brain. *J Neurosci Methods* **157**:71-81.
- Lowry OH, Rosebrough NJ, Farr AL, and Randall RJ (1951) Protein measurement with the Folin phenol reagent. *J Biol Chem* **193**:265-275.
- Maarouf CL, Walker JE, Sue LI, Dugger BN, Beach TG, and Serrano GE (2018) Impaired hepatic amyloid-beta degradation in Alzheimer's disease. *PLoS One* **13**:e0203659.
- Marques MA, Kulstad JJ, Savard CE, Green PS, Lee SP, Craft S, Watson GS, and Cook DG (2009) Peripheral amyloid-beta levels regulate amyloid-beta clearance from the central nervous system. *J Alzheimers Dis* **16**:325-329.
- Mawuenyega KG, Sigurdson W, Ovod V, Munsell L, Kasten T, Morris JC, Yarasheski KE, and Bateman RJ (2010) Decreased clearance of CNS beta-amyloid in Alzheimer's disease. *Science* **330**:1774 doi: 10.1126/science.1197623..

- Morris ME, Rodriguez-Cruz V, and Felmler MA (2017) SLC and ABC transporters: expression, localization, and species differences at the blood-brain and the blood-cerebrospinal fluid barriers. *AAPS J* **19**:1317–1331
- Nishida Y, Ito S, Ohtsuki S, Yamamoto N, Takahashi T, Iwata N, Jishage K, Yamada H, Sasaguri H, Yokota S, Piao W, Tomimitsu H, Saido TC, Yanagisawa K, Terasaki T, Mizusawa H, and Yokota T (2009) Depletion of vitamin E increases amyloid beta accumulation by decreasing its clearances from brain and blood in a mouse model of Alzheimer disease. *J Biol Chem* **284**:33400-33408.
- Pardridge WM (2016) CSF, blood-brain barrier, and brain drug delivery. *Expert Opin Drug Deliv* **13**:963-975.
- Pascale CL, Miller MC, Chiu C, Boylan M, Caralopoulos IN, Gonzalez L, Johanson CE, and Silverberg GD (2011) Amyloid-beta transporter expression at the blood-CSF barrier is age-dependent. *Fluids Barriers CNS* **8**:21.
- Poduslo JF, Curran GL, Sanyal B, and Selkoe DJ (1999) Receptor-mediated transport of human amyloid beta-protein 1-40 and 1-42 at the blood-brain barrier. *Neurobiol Dis* **6**:190-199.
- Qosa H, Abuasal BS, Romero IA, Weksler B, Couraud PO, Keller JN, and Kaddoumi A (2014) Differences in amyloid-beta clearance across mouse and human blood-brain barrier models: kinetic analysis and mechanistic modeling. *Neuropharmacology* **79**:668-678.
- Rao VV, Dahleimer JL, Bardgett ME, Snyder Az, Finch RA, Sartorelli AC, and Piwnicka-Worms D (1999) Choroid plexus epithelial expression of MDR1 P glycoprotein and multidrug resistance-associated protein contribute to the blood-cerebrospinal-fluid drug-permeability barrier. *Proc Natl Acad Sci USA* **96**:3900-3905.
- Roberts LM, Black DS, Raman C, Woodford K, Zhou M, Haggerty JE, Yan AT, Cwirla SE, and Grindstaff KK (2008) Subcellular localization of transporters along the rat blood-brain barrier and blood-cerebral-spinal fluid barrier by in vivo biotinylation. *Neuroscience* **155**:423-438.

- Roychaudhuri R, Zheng X, Lomakin A, Maiti P, Condrón MM, Benedek GB, Bitan G, Bowers MT, and Teplow DB (2015) Role of species-specific primary structure differences in Aβ₄₂ assembly and neurotoxicity. *ACS Chem Neurosci* **6**:1941-1955.
- Sagare A, Deane R, Bell RD, Johnson B, Hamm K, Pendu R, Marky A, Lenting PJ, Wu Z, Zarcone T, Goate A, Mayo K, Perlmutter D, Combs M, Zhong Z, and Zlokovic BV (2007) Clearance of amyloid-beta by circulating lipoprotein receptors. *Nat Med* **13**:1029-1031.
- Saido T and Leissring MA (2012) Proteolytic degradation of amyloid beta-protein. *Cold Spring Harbor Perspect Med* **2**:a006379.
- Saito Y, Buciak J, Yang J, and Pardridge WM (1995) Vector-mediated delivery of 125I-labeled beta-amyloid peptide Aβ₁₋₄₀ through the blood-brain barrier and binding to Alzheimer disease amyloid of the Aβ₁₋₄₀/vector complex. *Proc Natl Acad Sci U S A* **92**:10227-10231.
- Sakka L, Coll G, and Chazal J (2011) Anatomy and physiology of cerebrospinal fluid. *Eur Ann Otorhinolaryngol Head Neck Dis* **128**:309-316.
- Seppälä TT, Herukka SK, Hanninen T, Tervo S, Hallikainen M, Soininen H, and Pirttilä T (2010) Plasma Aβ₄₂ and Aβ₄₀ as markers of cognitive change in follow-up: a prospective, longitudinal, population-based cohort study. *J Neurol Neurosurg Psychiatry* **81**:1123-1127.
- Shibata M, Yamada S, Kumar SR, Calero M, Bading J, Frangione B, Holtzman DM, Miller CA, Strickland DK, Ghiso J, and Zlokovic BV (2000) Clearance of Alzheimer's amyloid-ss(1-40) peptide from brain by LDL receptor-related protein-1 at the blood-brain barrier. *J Clin Invest* **106**:1489-1499.
- Shiiki T, Ohtsuki S, Kurihara A, Naganuma H, Nishimura K, Tachikawa M, Hosoya K, and Terasaki T (2004) Brain insulin impairs amyloid-beta(1-40) clearance from the brain. *J Neurosci* **24**:9632-9637.
- Spies PE, Verbeek MM, van Groen T, and Claassen JA (2012) Reviewing reasons for the decreased CSF Aβ₄₂ concentration in Alzheimer disease. *Front Biosci (Landmark Ed)* **17**:2024-2034.

- Stine WB, Jr., Dahlgren KN, Krafft GA, and LaDu MJ (2003) *In vitro* characterization of conditions for amyloid-beta peptide oligomerization and fibrillogenesis. *J Biol Chem* **278**:11612-11622.
- Tamaki C, Ohtsuki S, Iwatsubo T, Hashimoto T, Yamada K, Yabuki C, and Terasaki T (2006) Major involvement of low-density lipoprotein receptor-related protein 1 in the clearance of plasma free amyloid beta-peptide by the liver. *Pharm Res* **23**:1407-1416.
- Tang C, Kuo Y, Pudvah NT, Ellis JD, Michener MS, Egbertson M, Graham SL, Cook JJ, Hochman JH, Prueksaritanont T (2009) Effect of P-glycoprotein-mediated efflux on cerebrospinal fluid concentrations in rhesus monkeys. *Biochem Pharmacol* **78**:642–647.
- Tarasoff-Conway JM, Carare RO, Osorio RS, Glodzik L, Butler T, Fieremans E, Axel L, Rusinek H, Nicholson C, Zlokovic BV, Frangione B, Blennow K, Menard J, Zetterberg H, Wisniewski T, and de Leon MJ (2015) Clearance systems in the brain-implications for Alzheimer disease. *Nat Rev Neurol* **11**:457-470.
- Takasawa A, Tetsuya T, Suzuki H, Ooie T, and Sugiyama Y (1997) Distributed model analysis of 3'-azido-3'-deoxythymidine and 2',3'-dideoxyinosine distribution in brain tissue and cerebrospinal fluid. *J Pharmacol Exp Ther* **282**:1509–1517.
- Teplov DB (2006) Preparation of amyloid beta-protein for structural and functional studies. *Methods Enzymol* **413**:20-33.
- Vergallo A, Megret L, Lista S, Cavedo E, Zetterberg H, Blennow K, Vanmechelen E, De Vos A, Habert MO, Potier MC, Dubois B, Neri C, Hampel H, group IN-ps, and Alzheimer Precision Medicine I (2019) Plasma amyloid beta 40/42 ratio predicts cerebral amyloidosis in cognitively normal individuals at risk for Alzheimer's disease. *Alzheimers Dement* **15**:764-775.
- Weidemann A, Paliga K, Dürrwang U, Reinhard FB, Schukert O, Evin G, and Masters CL (1999) Proteolytic processing of the Alzheimer's disease amyloid precursor protein within its cytoplasmic domain by caspase-like proteases. *J Biol Chem* **274**:5823–5829.

- Westerhout J, Ploeger B, Smeets J, Danhof M, and de Lange EC (2012) Physiologically based pharmacokinetic modeling to investigate regional brain distribution kinetics in rats. *AAPS J* **14**:543-553.
- Yamada K, Hashimoto T, Yabuki C, Nagae Y, Tachikawa M, Strickland DK, Liu Q, Bu G, Basak JM, Holtzman DM, Ohtsuki S, Terasaki T, and Iwatsubo T (2008) The low density lipoprotein receptor-related protein 1 mediates uptake of amyloid beta peptides in an *in vitro* model of the blood-brain barrier cells. *J Biol Chem* **283**:34554-34562.
- Yamamoto Y, Väitalo PA, Wong YC, Huntjens DR, Proost JH, Vermeulen A, Krauwinkel W, Beukers MW, Kokki H, Kokki M, Danhof M, van Hasselt JGC, de Lange ECM (2018) Prediction of human CNS pharmacokinetics using a physiologically-based pharmacokinetic modeling approach. *Eur J Pharm Sci* **112**:168-179
- Yasojima K, McGeer EG, and McGeer PL (2001) Relationship between beta amyloid peptide generating molecules and neprilysin in Alzheimer disease and normal brain. *Brain Res* **919**:115-121.
- Yasuda K, Cline C, Vogel P, Onciu M, Fatima S, Sorrentino BP, Thirumaran RK, Ekins S, Urade Y, and Schuetz EG (2013) Drug transporters on arachnoid barrier cells contribute to the blood-cerebrospinal fluid barrier. *Drug Metab Dispos* **41**:923-931.
- Zlokovic BV, Yamada S, Holtzman D, Ghiso J, and Frangione B (2000) Clearance of amyloid beta-peptide from brain: transport or metabolism? *Nat Med* **6**:718-719.

Footnotes

The work was supported by NSERC, the Natural Sciences and Engineering Research Council of Canada (KSP). H.B.P. was supported by the Dean's Scholarship Fund at the Leslie Dan Faculty of Pharmacy.

Figure Legends

Figure 1. Model I, II, and III are depicted in (A), (B), and (C) respectively, for the fitting of the plasma and CSF data after IV (intravenous) and ICV (intracerebroventricular) hA β ₄₀ administration.

Figure 2. Effect of plasma on suppressing absorbance signal (ODS) in the hA β ₄₀ ELISA assay, post dilution (A), with ODS prepared with different calibration standards in four different matrices (B), 50 μ L standard diluent buffer, SDB, 10 μ L plasma + 40 μ L SDB, undiluted rat plasma, or artificial CSF (aCSF), after sequential dilution with plasma or aCSF matrices to generate the calibration curves. The same colored symbol was used for standards prepared within the same calibration curve.

Figure 3. Rat plasma and CSF concentration-time profiles (concentrations normalized to dose, %dose·mL⁻¹) after IV administration of hA β ₄₀ to untreated ($n = 12$, left panels) and corn oil treated (q2d x4; right panels, $n = 4$) rats. Serial samples obtained from the same rat were denoted with the same symbol and color.

Figure 4. Prediction plots for Model I (upper panel), Model IA (middle panel, setting and $V_{1, \text{plasma}}$ and $V_{5, \text{CSF}}$ constant as those for Model I) and Model IB (bottom panel, setting and $V_{1, \text{plasma}}$, $V_{5, \text{CSF}}$ and k_{51} constant as those for Model I) after IV and ICV injections; serial samples obtained from the same rat were denoted with the same symbol. The black line represents the line of identity.

Figure 5. Fits of observed versus predicted plasma and CSF concentrations in control and calcitriol treated rats after hA β ₄₀ IV and ICV administration (data of Figure 4) to Model I. The red and blue lines represent the lines of best fit for plasma and CSF, respectively, and the shaded regions denote the 5% and 95% confidence interval. Serial samples obtained from the same rat were denoted with the same symbol.

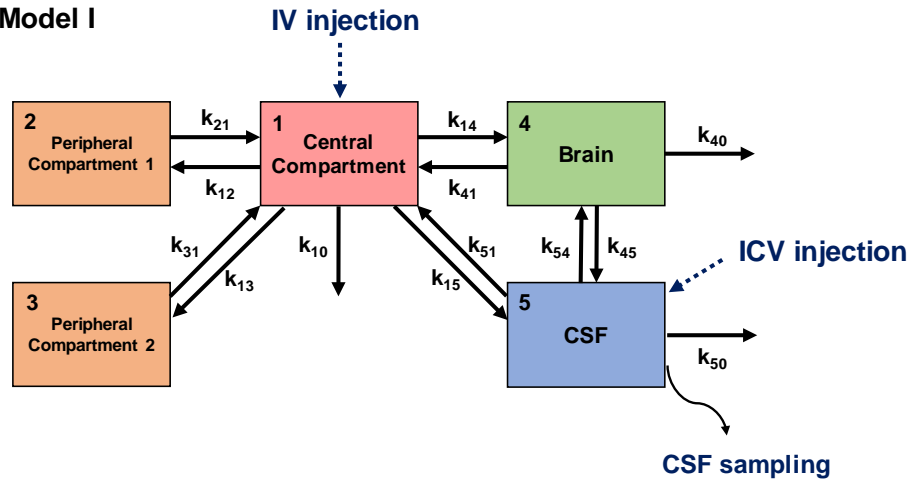
Figure 6. Simulations based on fitted parameters for Model I (Table 3) >800 min for plasma, brain, and CSF concentrations after hA β ₄₀ was given as single IV and ICV injections, with and without calcitriol treatment.

Figure 7. Relative brain P-gp, neprilysin (Nep), Lrp1 and Mrp1 protein expressions in corn oil-treated control and calcitriol-treated rats, determined by Western Immunoblotting, were presented. The background-corrected signals of P-gp (170 kDa) and neprilysin (85.5 kDa) in the same sample were separated on the same gel and normalized to the intensity of the house-keeping gene, Gapdh (36 kDa). Separate gels were individually used for the determination of Lrp1 (85 kDa) and Mrp1 (172 kDa). * $P < 0.05$ denotes significance.

Figure 1

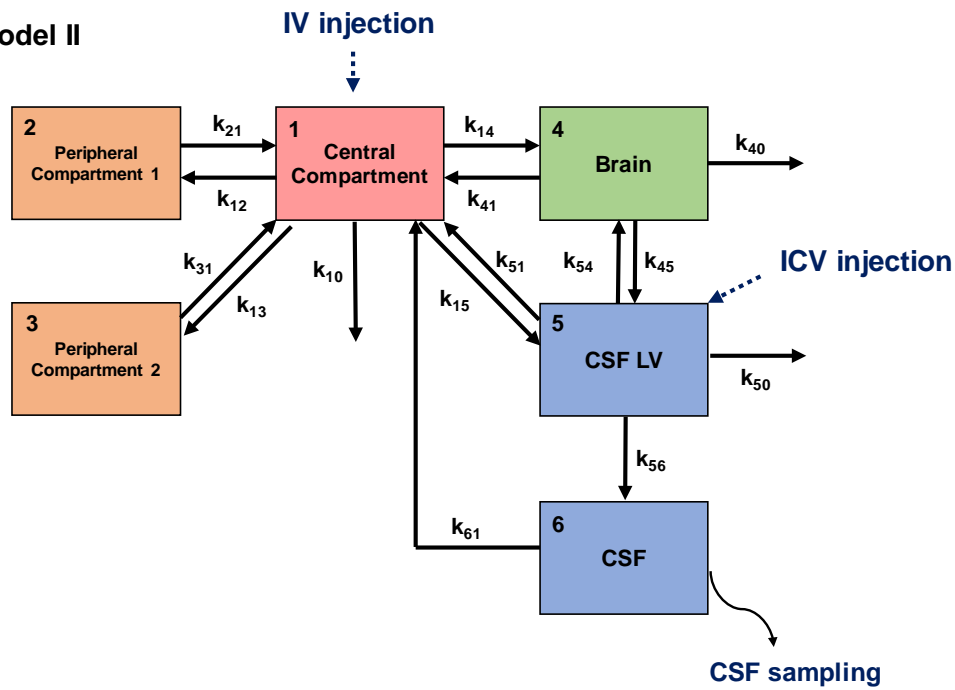
(A)

Model I



(B)

Model II



(C)

Model III

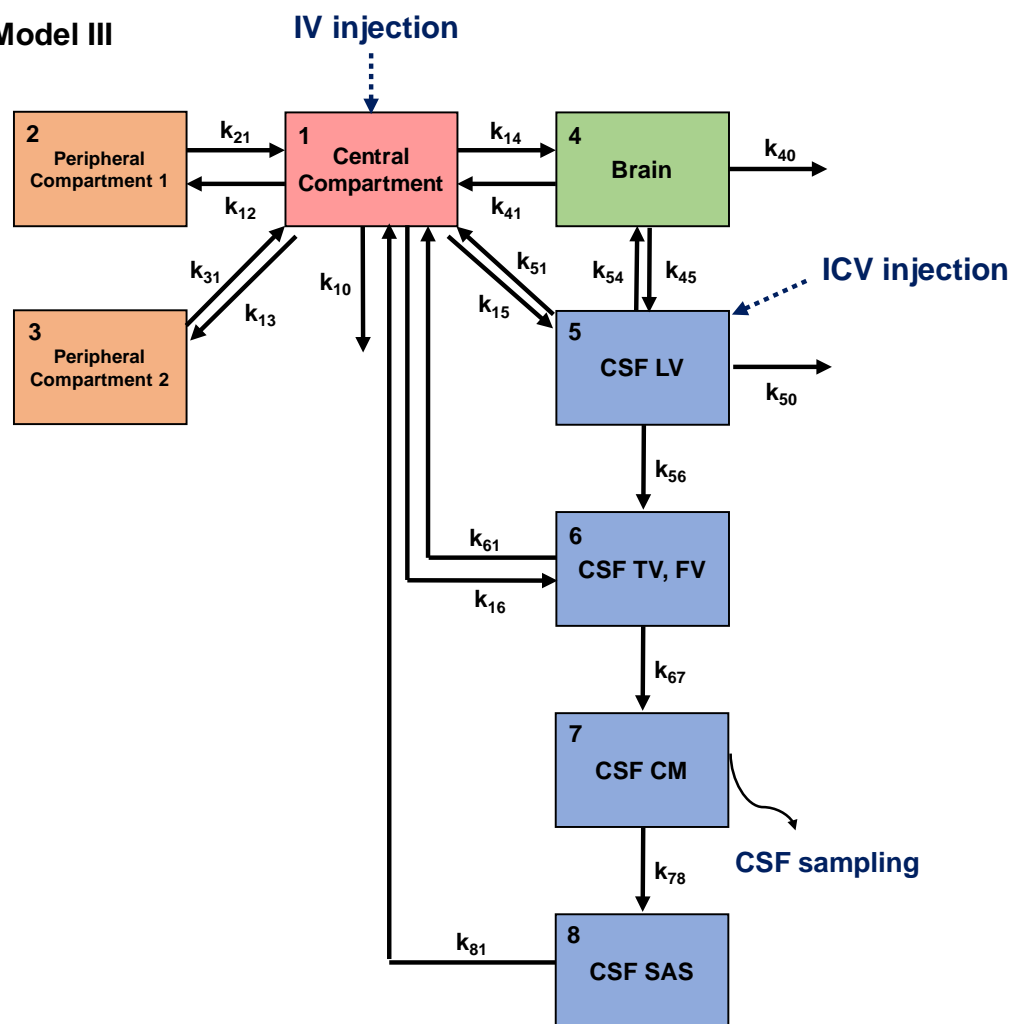


Figure 2

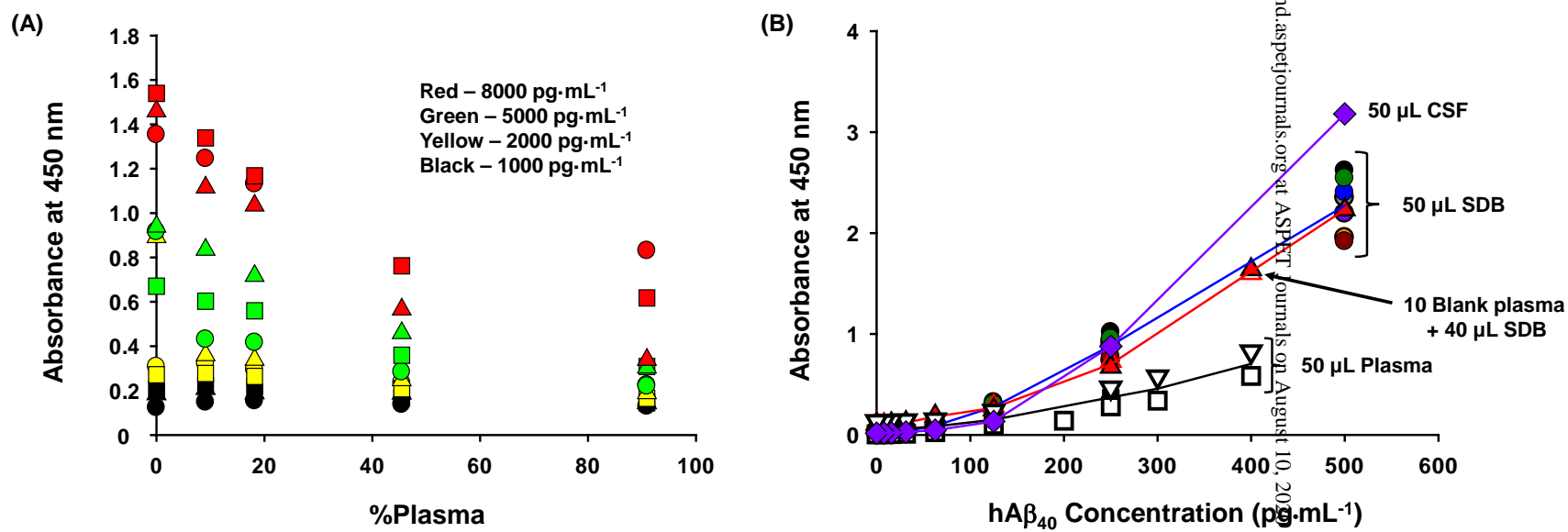


Figure 3

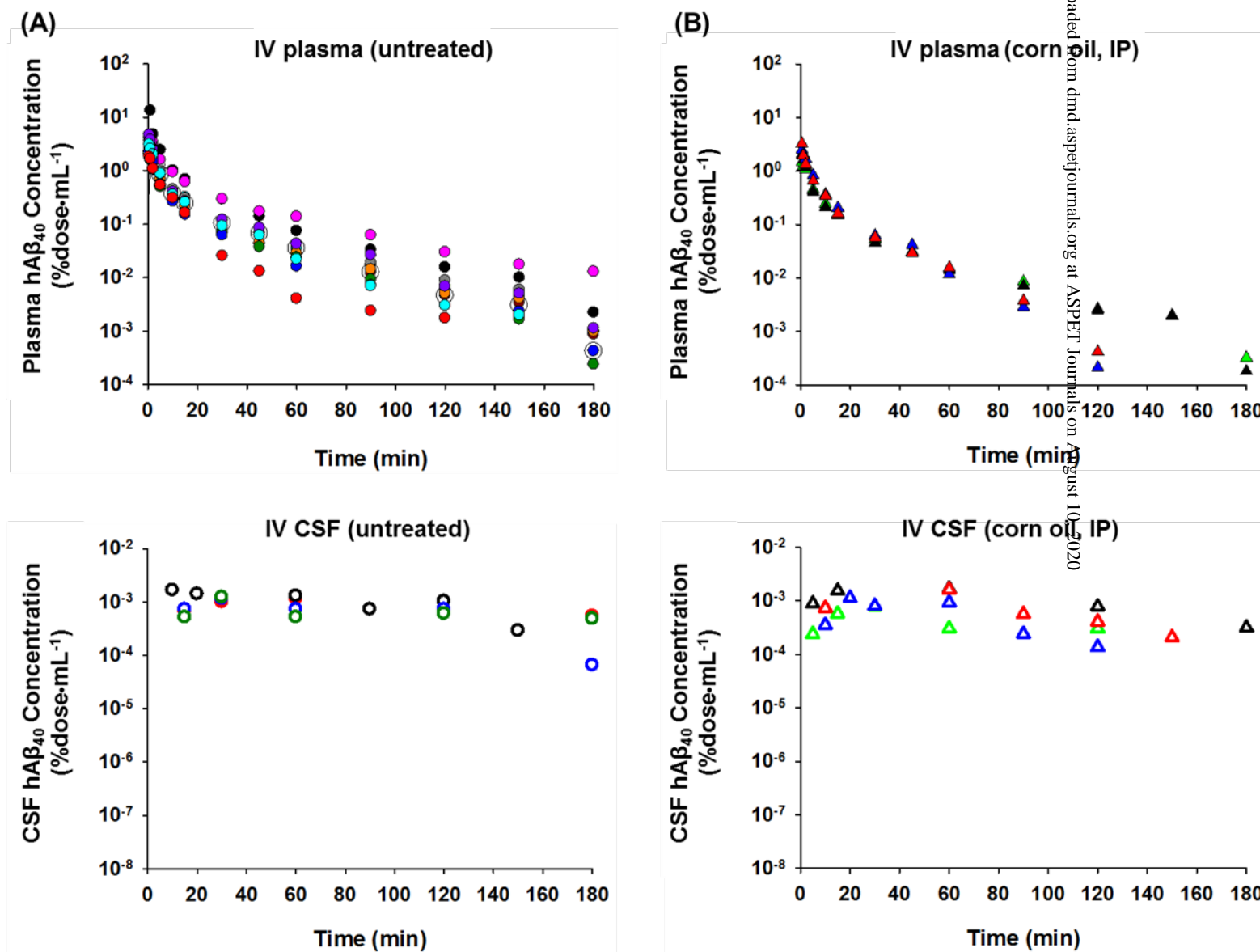
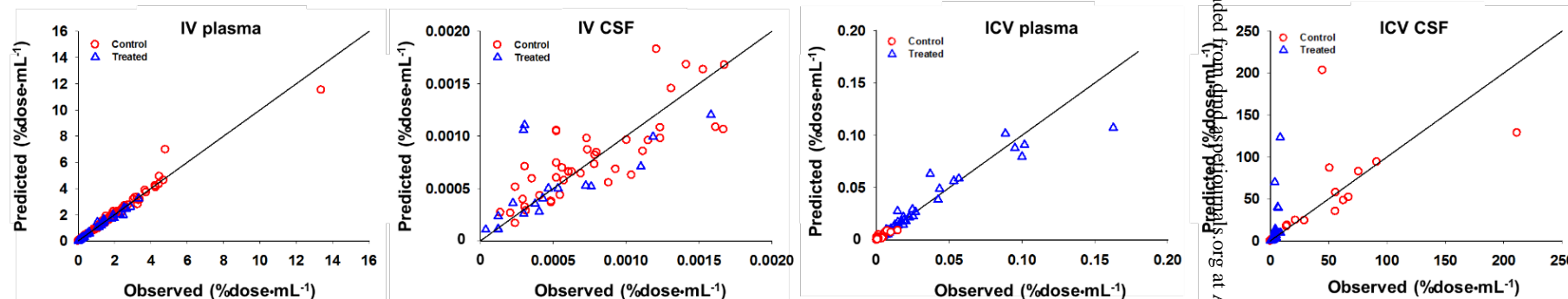
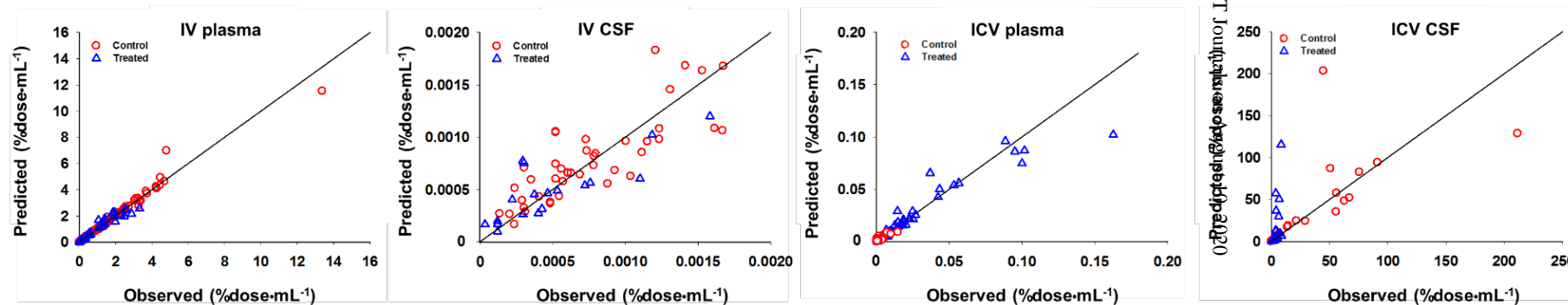


Figure 4.

Model I



Model IA



Model IB

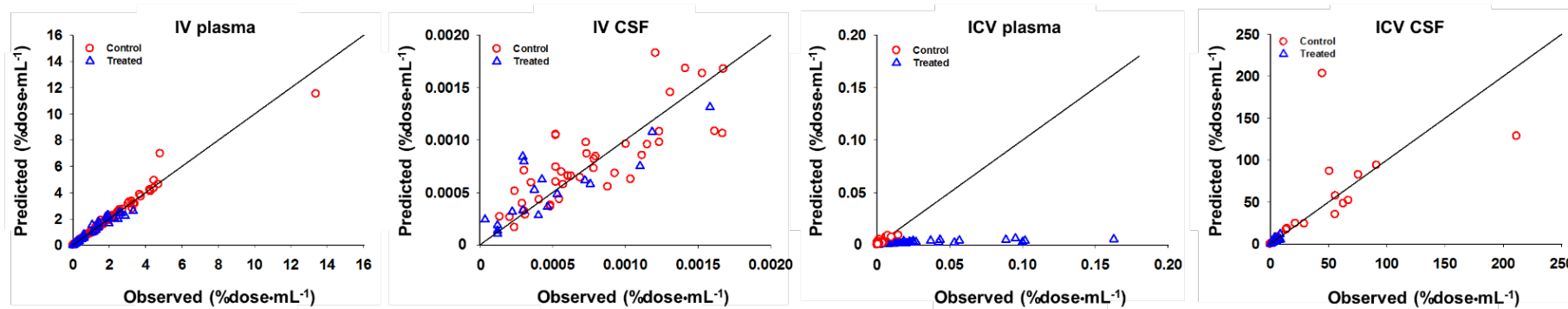


Figure 5

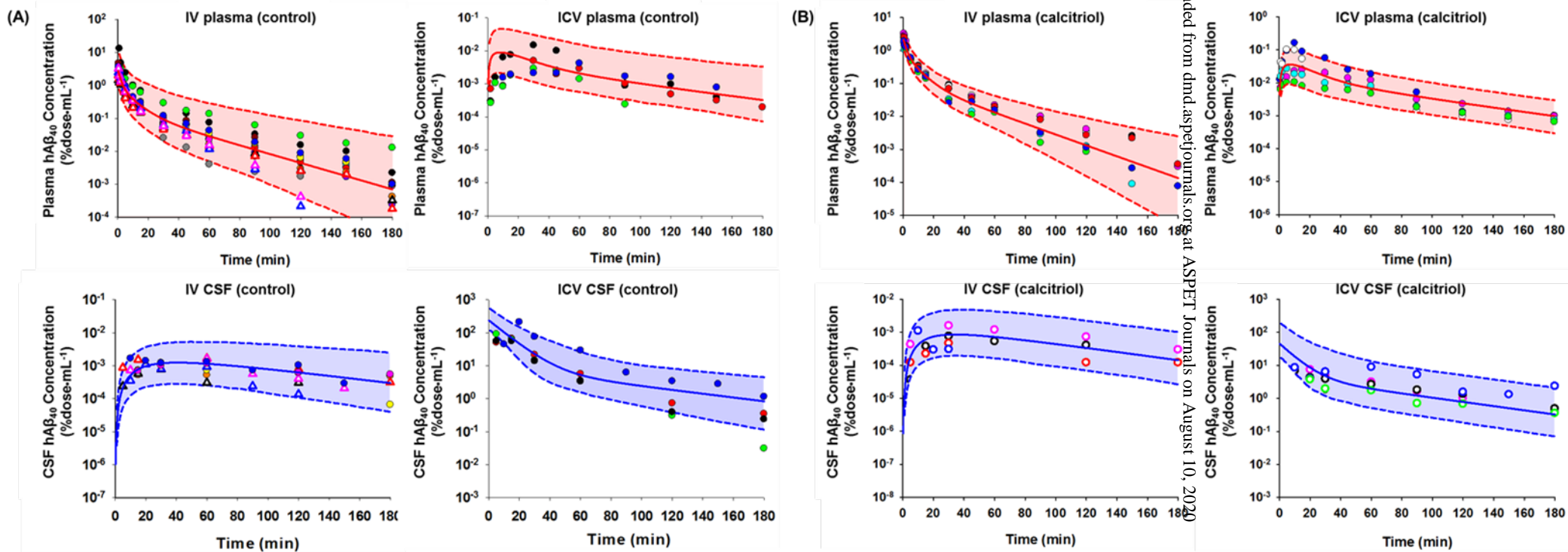


Figure 6

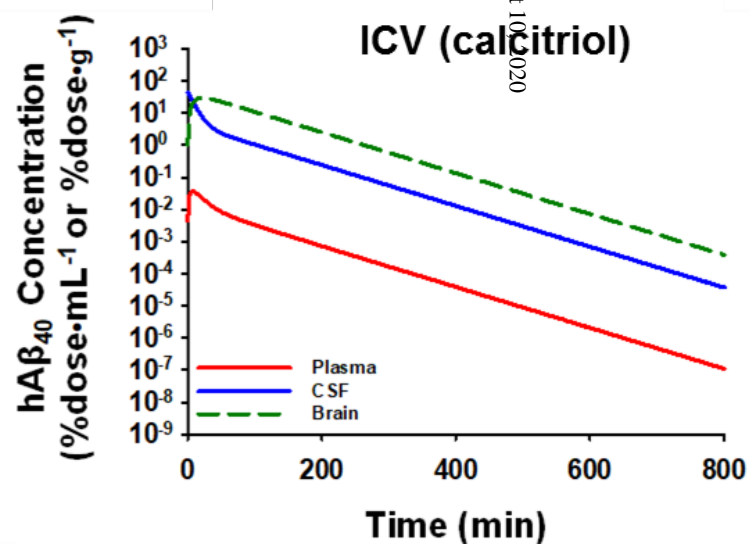
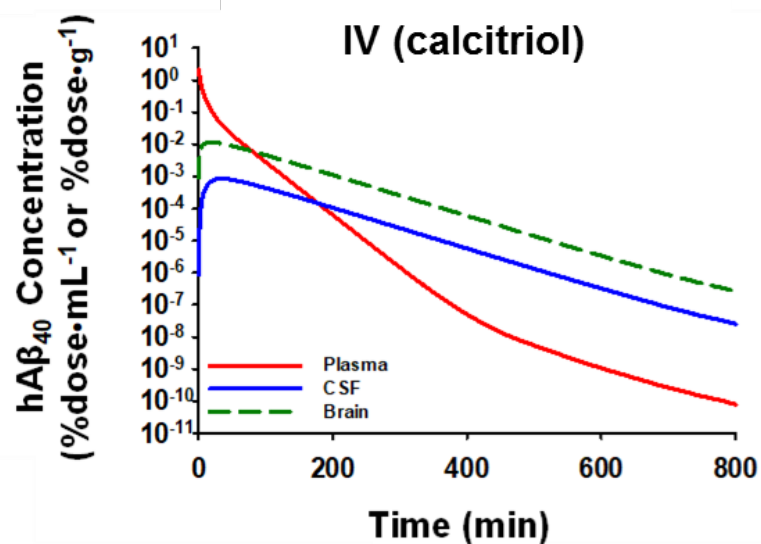
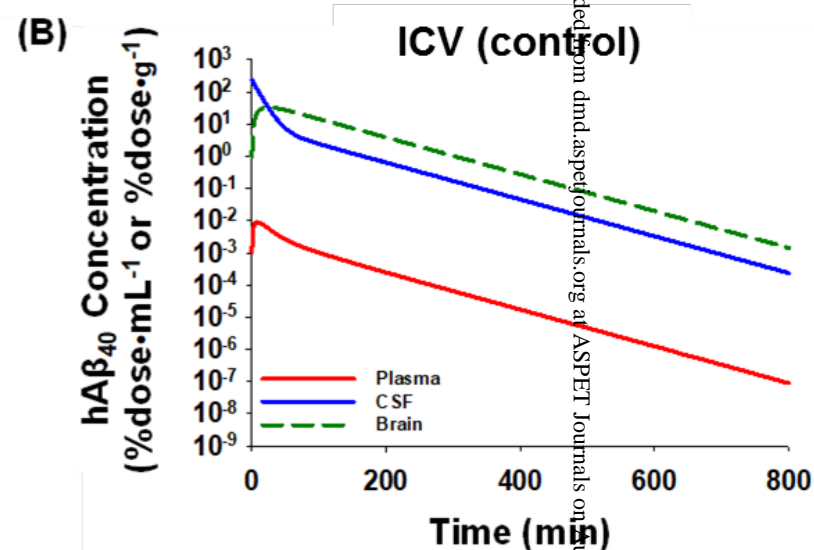
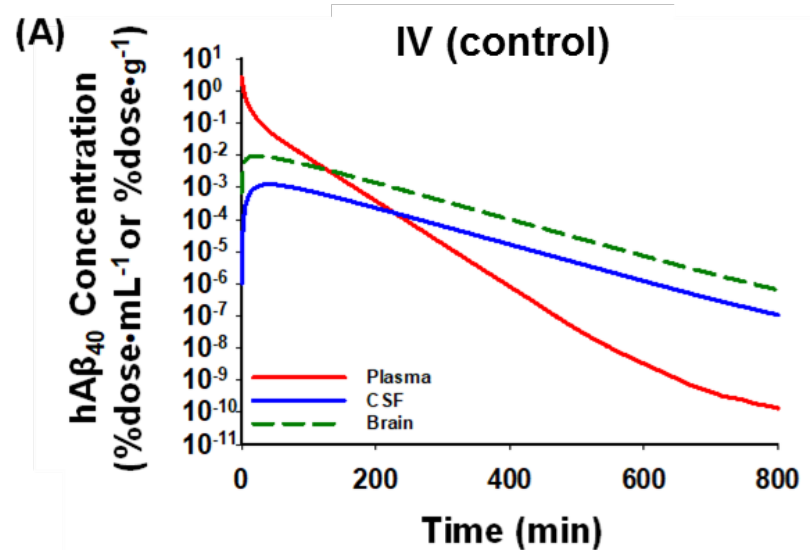


Figure 7

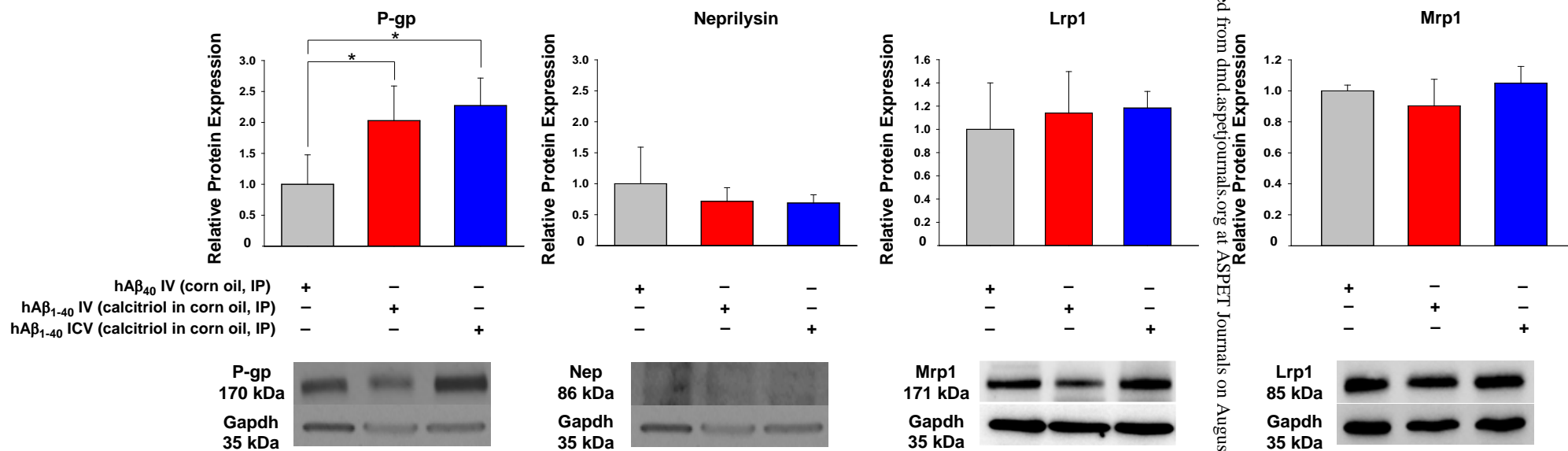


Table 1. Non-compartmental parameters for hA β ₄₀ after single IV injections to untreated and IP corn oil treated rats (absence of calcitriol treatment)^a

Parameter	Without Calcitriol Treatment		<i>P</i> value
	IV hA β ₄₀ (<i>n</i> = 12)	IV hA β ₄₀ & corn oil (IP) (<i>n</i> = 4)	
Rat weight (g)	282 ± 24.9	339 ± 76.2	<i>NS</i> ^b
dose (μg·kg ⁻¹)	64.5 ± 13.2	68.5 ± 12.0	<i>NS</i>
AUC _{0-∞,plasma} (%dose·min·mL ⁻¹) ^c	24.2 ± 14.7	13.2 ± 2.56	<i>NS</i>
AUC _{0-∞,CSF} (%dose·min·mL ⁻¹) ^c	0.121 ± 0.040	0.124 ± 0.063	<i>NS</i>
Observed t _{1/2,terminal plasma} (min)	24.5 ± 4.05	16.8 ± 5.66	<i>NS</i>
Observed t _{1/2,terminal CSF} (min)	75.5 ± 17.9	47.9 ± 20.9	<i>NS</i>
CL _{plasma} (mL·min ⁻¹ ·kg ⁻¹)	17.9 ± 6.20	23.2 ± 2.21	<i>NS</i>
CL _{bile} = f _{bile} · CL _{plasma} (mL·min ⁻¹ ·kg ⁻¹)	0.00161 ± 0.00124	<i>ND</i> ^d	<i>NA</i> ^e
$K_{p,CSF:plasma} = \frac{AUC_{CSF}}{AUC_{plasma}}$	0.0085 ± 0.0021	0.0099 ± 0.0068	<i>NS</i>

^aMean ± S.D

^bNot significant; *P* > 0.05

^cAUC_{0-∞} (AUC_{0-180min} by trapezoidal rule + C_{180min}/terminal phase rate constant)

^dNot determined

^eNot applicable

Downloaded from https://academic.oup.com/aspetjournals.org at ASPET Journals on August 10, 2020

Table 2. The WSSR and AIC for control data sets vs. the calcitriol treated data for the fitted compartment models (shown in Figure 1)

Model	Description	Statistic Parameters			
		Control ^a		Calcitriol-Treated	
		WSSR ^b	AIC ^c	WSSR	AIC
I	Set $k_{15}=0$ for control and treatment groups; no constraints for volumes	225	-1429	170	-794
IA	Set $k_{15}=0$ (same as Model I); assign fitted $V_{1,\text{plasma}}$ & $V_{5,\text{CSF}}$ estimates from control data fit to the treatment group	225	-1429	178	-810
IB	Set $k_{15}=0$ (same as Model I); assign fitted $V_{1,\text{plasma}}$, $V_{5,\text{CSF}}$, & k_{51} estimates from control data fit to the treatment group	225	-1429	173	-454
II	Set k_{15} & $k_{51}=0$ for control and treatment groups; no constraints for volumes	230	-1361	173	-628
IIA	Set k_{15} & $k_{51}=0$ (same as Model II); assign fitted $V_{1,\text{plasma}}$ & $V_{6,\text{CSF}}$ estimates from control data fit to the treatment group	230	-1361	170	-485
IIB	Set k_{15} & $k_{51}=0$ (same as Model II); assign fitted $V_{1,\text{plasma}}$, $V_{6,\text{CSF}}$, k_{56} , & k_{61} estimates from control data fit to the treatment group	230	-1361	171	-198
III	Set k_{15} , k_{16} , k_{51} & $k_{61}=0$ for control and treatment groups; no constraints for volumes	227	-1292	176	-261
IIIA	Set k_{15} , k_{16} , k_{51} & $k_{61}=0$ (same as Model III); assign fitted $V_{1,\text{plasma}}$ & $V_{7,\text{CM}}$, estimates from control data fit to the treatment group	227	-1292	184	-229
IIIB	Set k_{15} , k_{16} , k_{51} & $k_{61}=0$ (same as Model III); assign fitted $V_{1,\text{plasma}}$, $V_{7,\text{CM}}$, k_{56} , k_{67} , k_{78} , & k_{81} estimates from control data fit to the treatment group	227	-1292	187	-307

^a F score for the fitted control data sets for Models I, II and III (and the A and B versions) were calculated, was calculated as $\left[\frac{(SSR_j - SSR_i)}{SSR_i} \right] \times \left[\frac{df_i}{(df_j - df_i)} \right]$, where $df_j > df_i$; and was compared to the critical F value, obtained from the F table with the numerator as $df_j - df_i$ and denominator as df_i . The F score was compared to the critical F value with significance level $\alpha = 0.05$. The scores for the control and calcitriol data were not significant versus Model I (data not shown).

^bWSSR was provided by ADAPT5®

^cAIC, a measurement of the goodness-of-fit, provided by ADAPT5®

Table 3. MLEM population parameters for simultaneous fit of IV and ICV hA β_{40} data with Models I, IA, and IB (k_{15} assigned as 0) with fitting by ADAPT5[®]

Population Fitted Parameters ^a	Control Rats – Fit 1		Calcitriol Treated Rats – Fit 2	
	Model I		Model IA	
	IV (n = 16 ^b) & ICV (n = 4)	IV (n = 7) & ICV (n = 5)	V _{1,plasma} & V _{5,CSF} same as Model I IV (n = 7) & ICV (n = 5)	V ₁ , V ₅ & k_{51} same as Model I IV (n = 7) & ICV (n = 5)
k_{10} (min ⁻¹)	0.186 ± 0.0901	0.206 ± 0.0335	0.176 ± 0.0823	0.231 ± 0.0506
k_{12} (min ⁻¹)	0.164 ± 0.0416	0.140 ± 0.0575	0.195 ± 0.0796	0.141 ± 0.112
k_{13} (min ⁻¹)	0.0524 ± 0.0255	0.0426 ± 0.0207	0.0479 ± 0.0133	0.0468 ± 0.00727*
k_{14} (min ⁻¹)	0.0000523 ± 0.0000172	0.0000690 ± 0.0000229*	0.0000605 ± 0.0000232	0.0000868 ± 0.0000411*
k_{21} (min ⁻¹)	0.245 ± 0.0942	0.271 ± 0.132	0.367 ± 0.216*	0.279 ± 0.0920
k_{31} (min ⁻¹)	0.0430 ± 0.0120	0.0492 ± 0.0196	0.0603 ± 0.0322	0.0415 ± 0.00437
k_{40} (min ⁻¹)	0.0131 ± 0.00619	0.0139 ± 0.00311	0.0148 ± 0.00389	0.0124 ± 0.00278
k_{41} (min ⁻¹)	0.000105 ± 0.0000287	0.000188 ± 0.0000302*	0.000181 ± 0.0000600*	0.000131 ± 0.0000318*
k_{45} (min ⁻¹)	0.00274 ± 0.00154	0.00938 ± 0.00446*	0.00439 ± 0.00167*	0.00754 ± 0.00513*
k_{50} (min ⁻¹)	0.0110 ± 0.00117	0.0114 ± 0.00126	0.0137 ± 0.00168*	0.0117 ± 0.00132*
k_{51} (min ⁻¹)	0.00146 ± 0.000787	0.00791 ± 0.00548*	0.0120 ± 0.00841*	0.00146 (fixed)
k_{54} (min ⁻¹)	0.0722 ± 0.0154	0.0754 ± 0.0472	0.180 ± 0.124*	0.435 ± 0.187*
V _{1,plasma} (mL)	33.1 ± 26.7	42.4 ± 15.2	33.1 (fixed)	33.1 (fixed)
V _{5,CSF} (mL)	0.417 ± 0.203	2.20 ± 1.84*	0.417 (fixed)	0.417 (fixed)
CL _{plasma} = $k_{10} \cdot V_{1,plasma}$ (mL·min ⁻¹ ·kg ⁻¹)	21.8	25.8*	17.2	22.6

^aMean ±S.D. (CV%) of parameter estimate

^bPooled IV injected mice (with or without corn oil injections, n=16)

* $P < 0.05$, Wilcoxon rank sum test (nonparametric test, conducted in R); from individual fits (data not shown)

Table 4. Simulated $AUC_{0-\infty}$ for plasma, brain and CSF to yield partition coefficients (K_p) based on fitted parameters with Model I (Table 3) for calcitriol-treated and control rats

	Control – Fit 1 (untreated)		Treatment - Fit 2 (calcitriol in corn oil IP)		Ratio (Treated/Control)	
	IV	ICV	IV	ICV	IV	ICV
$AUC_{\infty, \text{plasma}} (\% \text{dose} \cdot \text{min} \cdot \text{mL}^{-1})$	16.2	0.435	11.4	1.52	0.70	3.49
$AUC_{\infty, \text{brain}} (\% \text{dose} \cdot \text{min} \cdot \text{mL}^{-1})$	1.14	3482	1.17	2812	1.03	0.81
$AUC_{\infty, \text{CSF}} (\% \text{dose} \cdot \text{min} \cdot \text{mL}^{-1})$	0.159	3319	0.095	709	0.597	0.214
$K_{p, \text{brain:plasma}} = \frac{AUC_{\infty, \text{brain}}}{AUC_{\infty, \text{plasma}}}$	0.0700	8007	0.102	1847	1.45	0.231
$K_{p, \text{CSF:plasma}} = \frac{AUC_{\infty, \text{CSF}}}{AUC_{\infty, \text{plasma}}}$	0.00983	7633	0.00827	466	0.842	0.051
$\frac{AUC_{\infty, \text{CSF}}}{AUC_{\infty, \text{brain}}}$	0.140	0.953	0.0811	0.252	0.58	0.264

Downloaded from dm.aspetjournals.org at ASPET Journals on August 10, 2020